High-energy neutrino astronomy

We expect νs from astrophysical sources like AGN at TeV / PeV energies

(above solar νs & atmospheric νs)

fluxes are extremely small

=> even bigger detectors

water / ice Čerenkov detectors

e.g. Antares Mediterranian Sea

Ice Cube South Pole

Neutrino Flux

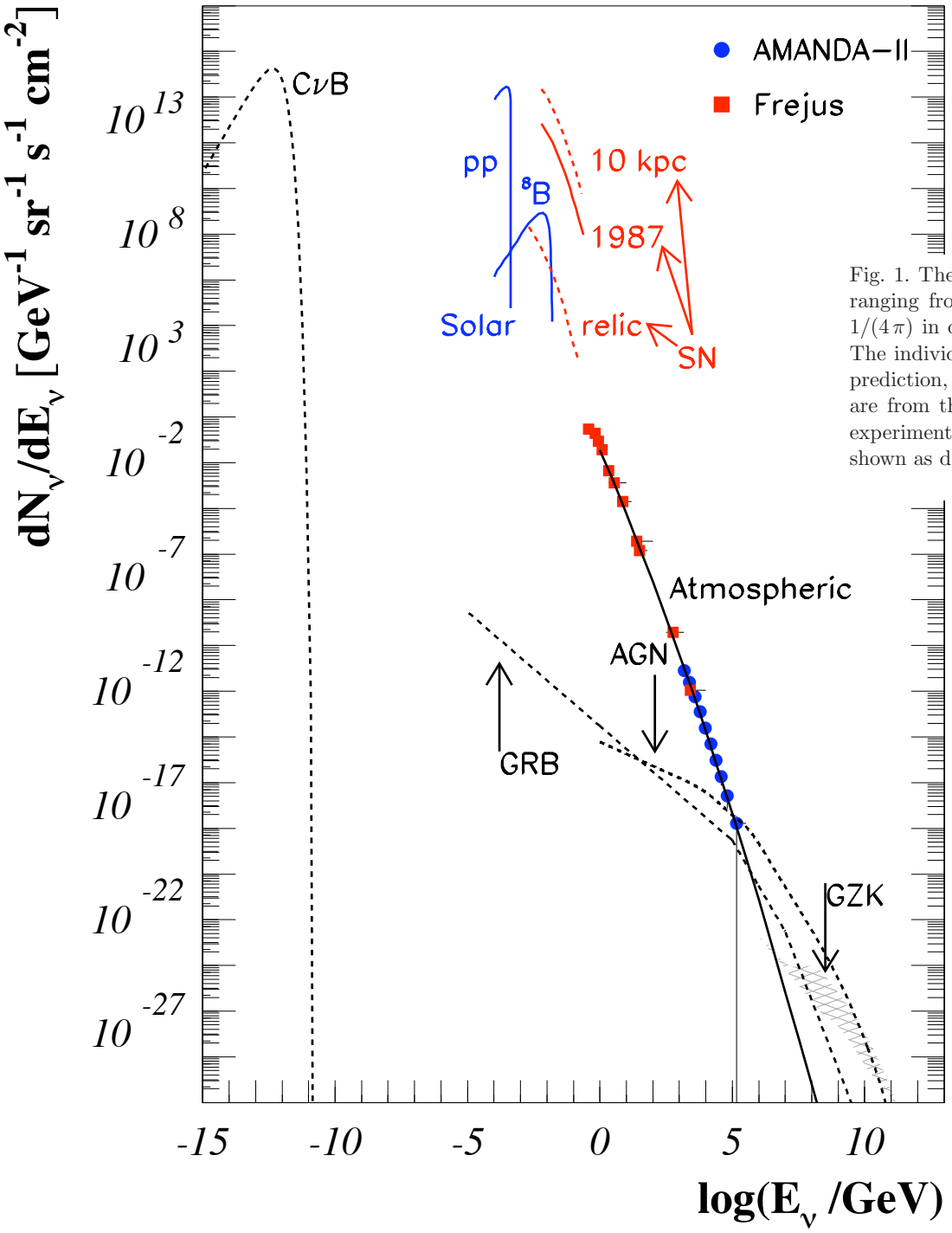

Fig. 1. The astrophysical neutrino spectrum including different source predictions ranging from meV up to EeV energies. Point source fluxes have been scaled by $1/(4\pi)$ in order to be comparable to diffuse spectra. Figure after [Kos92, Rou00]. The individual spectra are explained and referenced in the text. The atmospheric prediction, averaged over the solid angle, is taken from [Vol80], the atmospheric data are from the FRÉJUS experiment [D$^+$95] (red squares) and from the AMANDA experiment (blue circles) [M$^+$07, Mün07]. The fluxes based on mere predictions are shown as dashed lines. The solid lines represent those fluxes already measured.

J. Becker arXiv:0710.1557

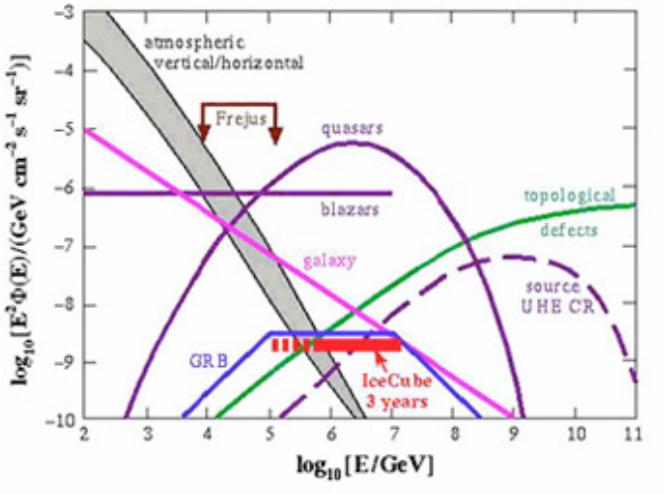

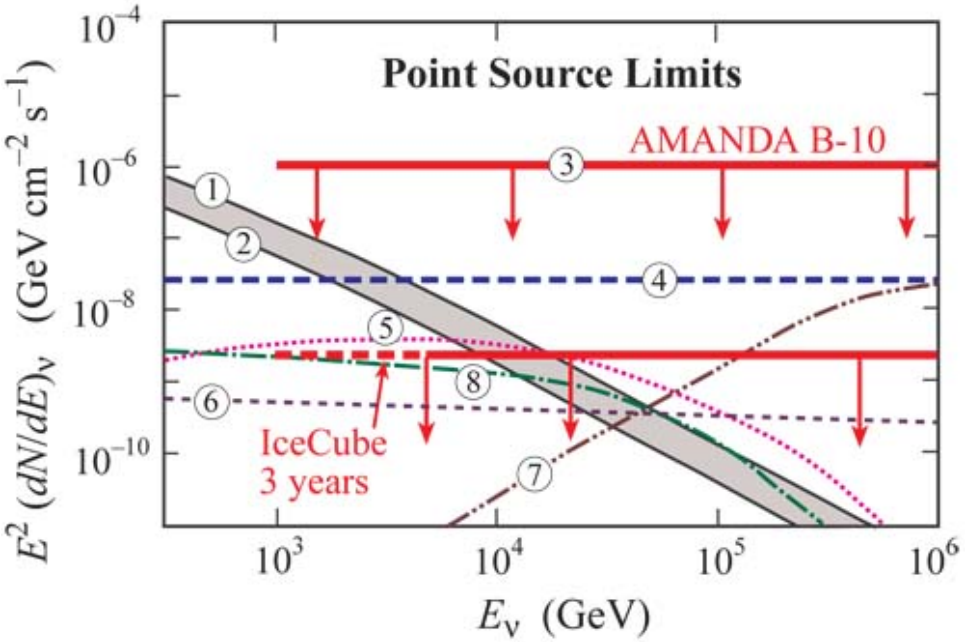

Predictions of high energy $\nu_\mu + \nu_\mu$ fluxes from astrophysical sources are shown. Also shown are the preliminary average upper limit as obtained with AMANDA-B10 (3), as well as the sensitivity of the proposed IceCube array after three years of operation. The atmospheric neutrino flux [59] in 2 × 2 degree bin is given as reference: (1) horizontal, (2) vertical. Models: (4) 3C273 pp neutrinos [60], (5) Crab Nebula [61], (6) Coma Cluster [62], (7) 3C273 pγ neutrinos [63], (8) Supernova IC443 [64].

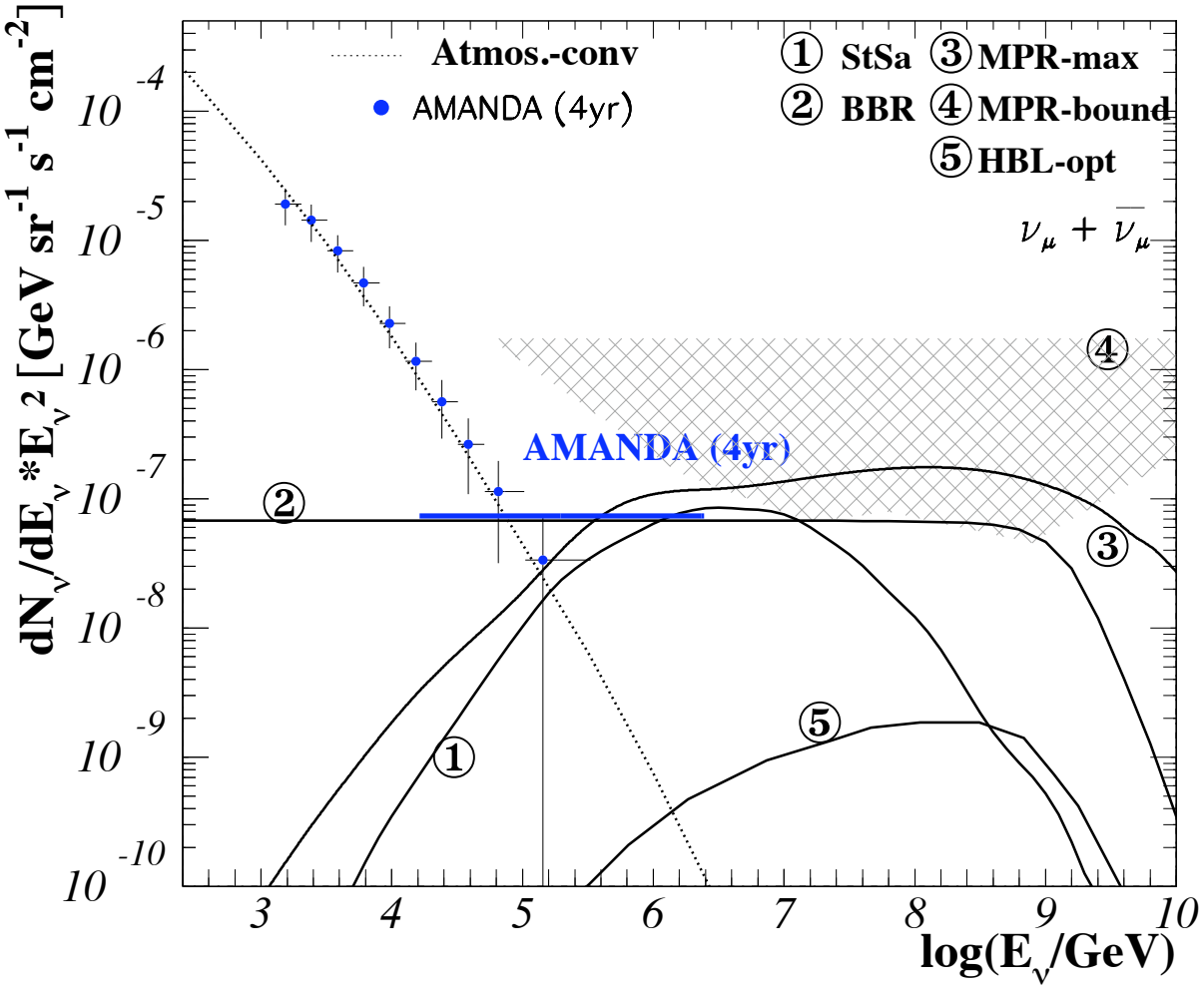

Fig. 20. AGN neutrino flux models: ① ν-MeV correlation for blazars [Ste05]; ② ν-radio correlation for FR-II galaxies & FSQRs [BBR05a], using an optical depth of $\tau = 0.2$; ③ maximum contribution from EGRET sources [MPR01]; ④ upper bound for νs from optically thick sources (upper, straight bound) and from optically thin sources (lower, curved bound of shaded area) [MPR01]; ⑤ Optimum prediction for High-peaked BL Lacs (HBL-opt) within the proton-blazar model [M$^+$03b]. The atmospheric prediction is shown as the dotted line [Vol80], data are for four years of AMANDA-II data [M$^+$07, Mün07], as well as the limit given in [AI$^+$07d].

J. Becker arXiv:0710.1557

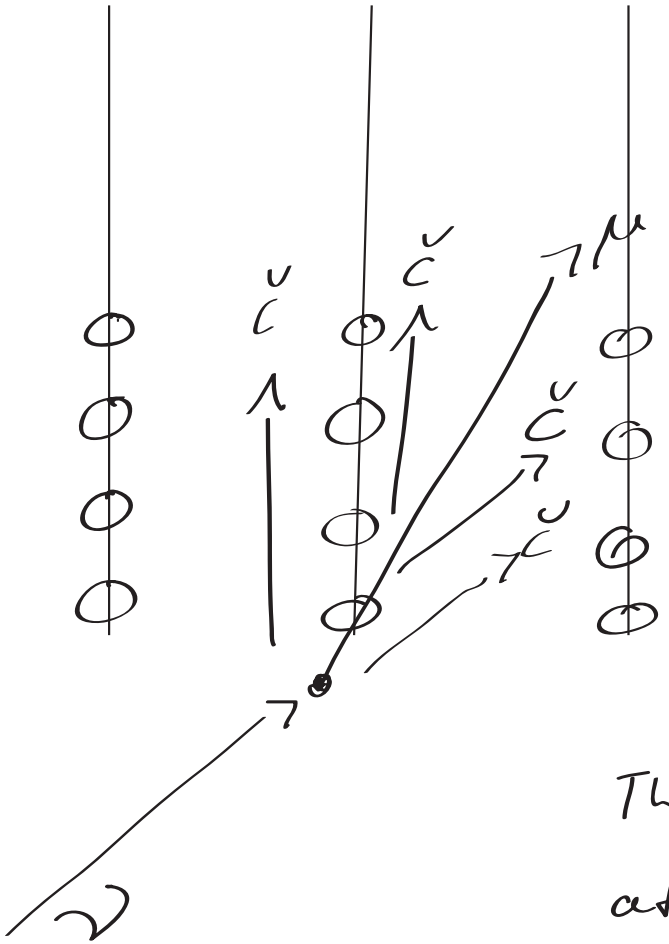

water / ice

chains of PMTs
are deployed
in water / ice

~ 2 km
deep

The detectors measure
atmospheric ν
but so far no νs from
astrophysical sources
rumors from Ice Cube

ANTARES

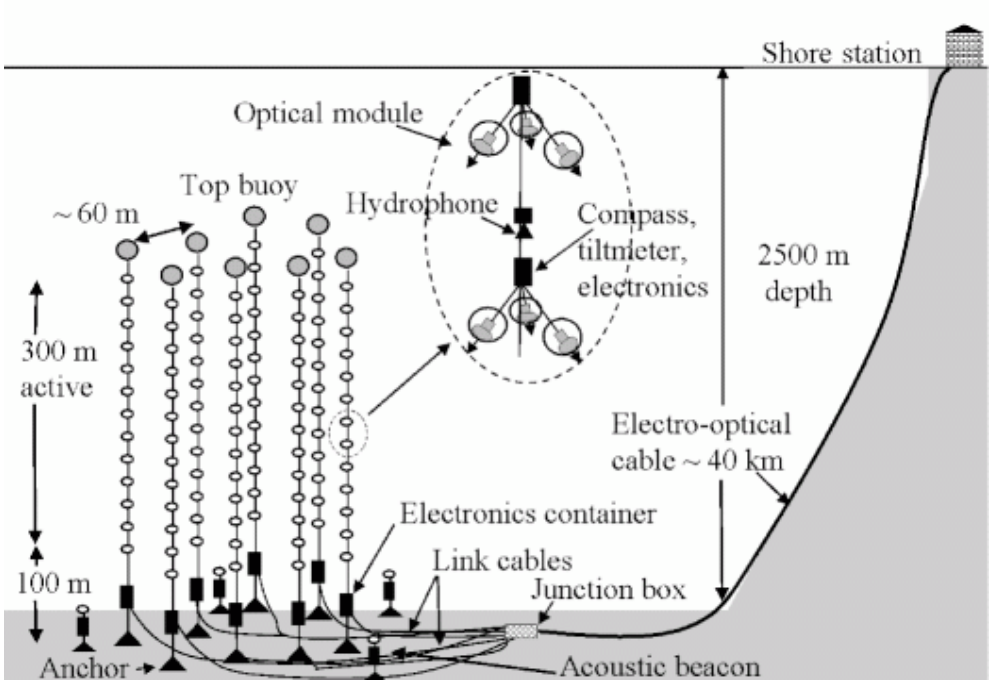
Shore station
Optical module
Top buoy
Hydrophone
~60 m
Compass,
tiltmeter,
electronics
2500 m
depth
300 m
active
Electro-optical
cable ~ 40 km
Electronics container
Link cables
100 m
Junction box
Anchor
Acoustic beacon

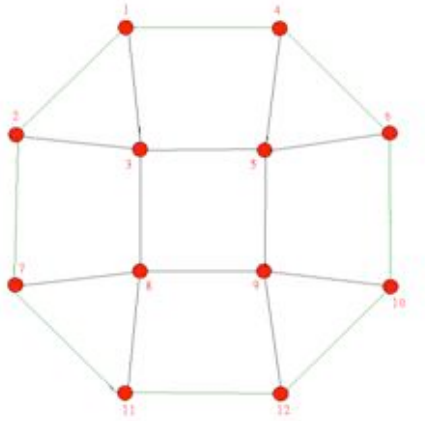

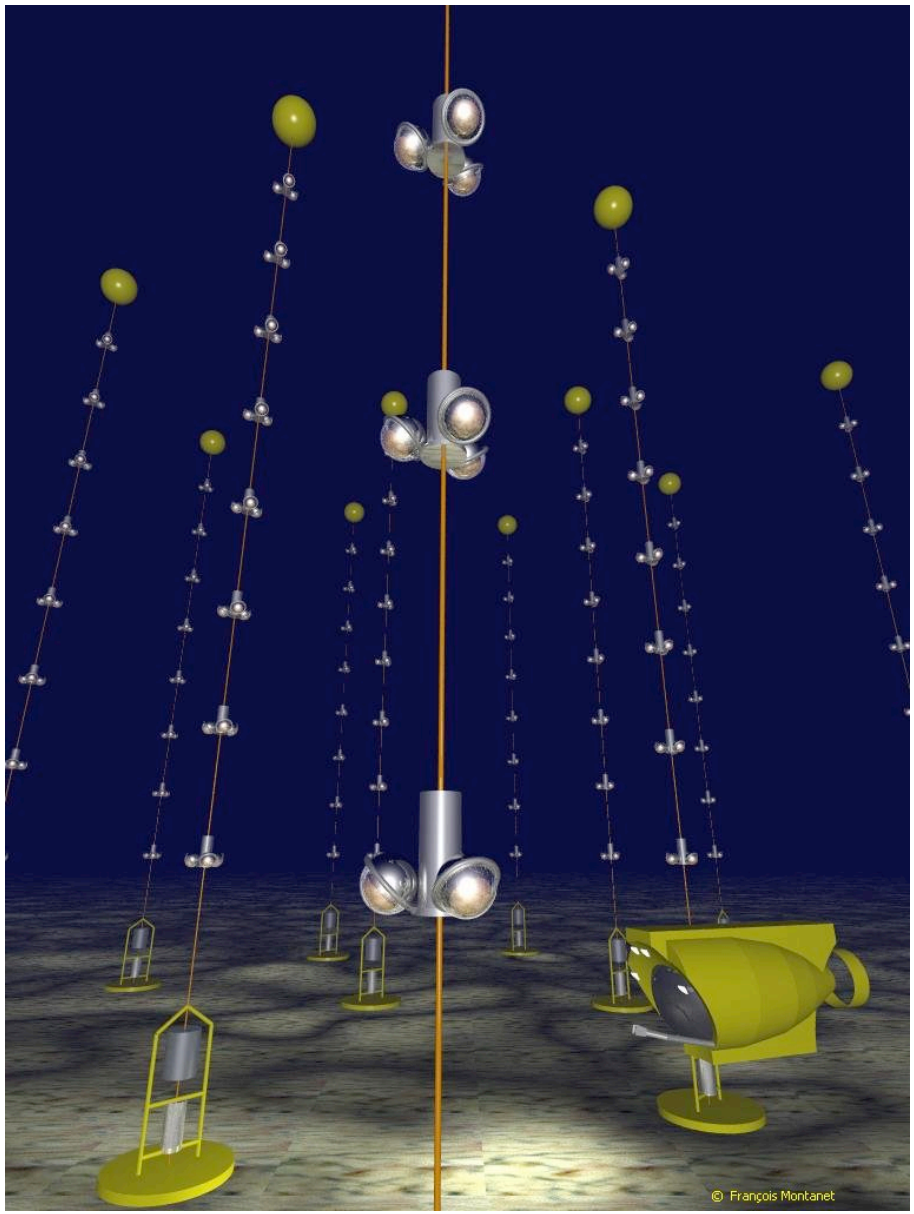
© François Montanet

ANTARES

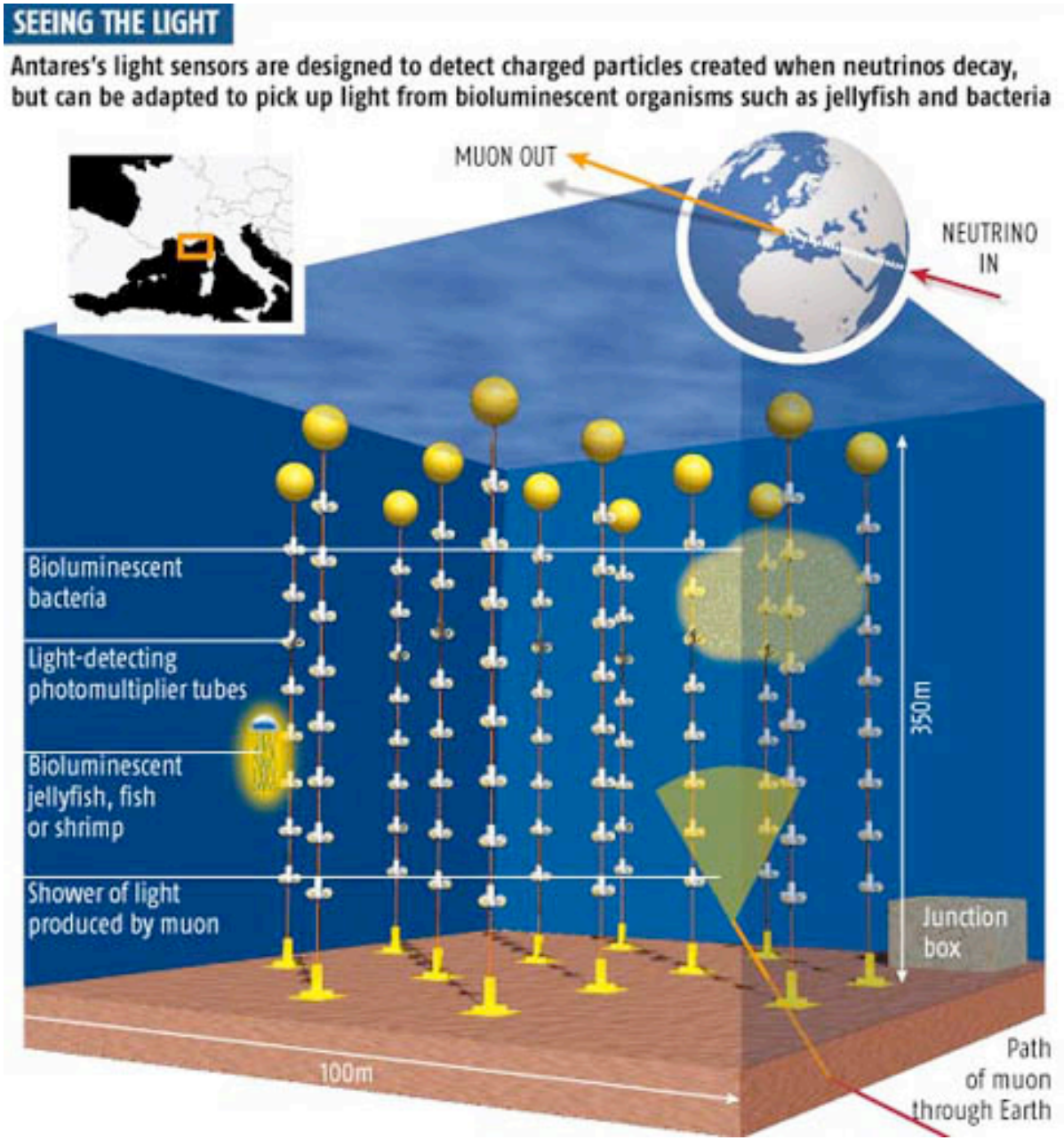
SEEING THE LIGHT
Antares's light sensors are designed to detect charged particles created when neutrinos decay, but can be adapted to pick up light from bioluminescent organisms such as jellyfish and bacteria
MUON OUT
NEUTRINO IN
Bioluminescent bacteria
Light-detecting photomultiplier tubes
Bioluminescent jellyfish, fish or shrimp
Shower of light produced by muon
350m
Junction box
100m
Path of muon through Earth

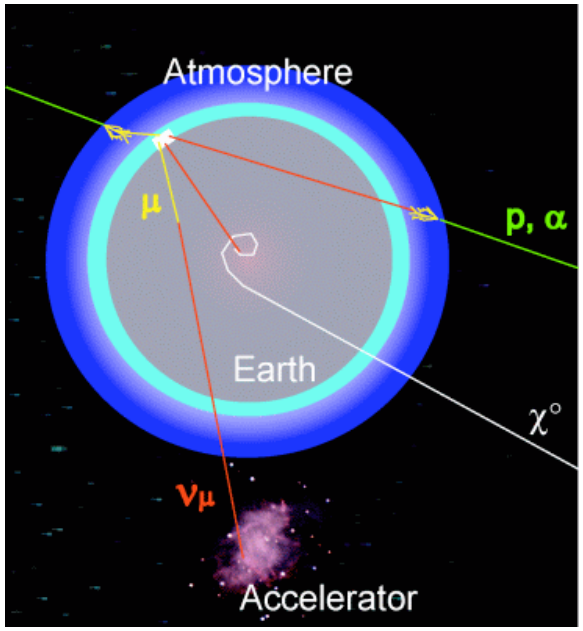
Atmosphere
μ
p, α
Earth
χ°
νμ
Accelerator

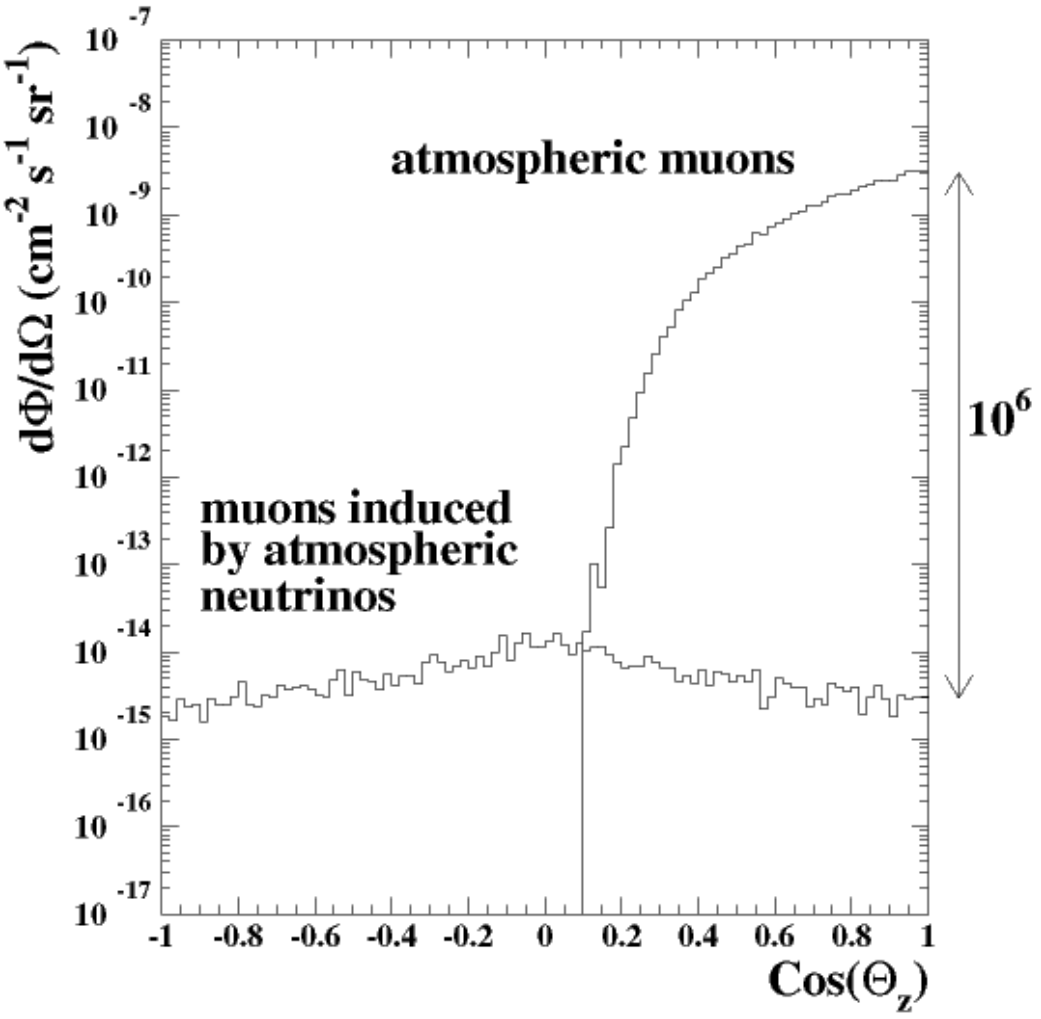
atmospheric muons
muons induced by atmospheric neutrinos
10^6
dΦ/dΩ (cm^-2 s^-1 sr^-1)
Cos(Θz)
10^-7
10^-8
10^-9
10^-10
10^-11
10^-12
10^-13
10^-14
10^-15
10^-16
10^-17
-1
-0.8
-0.6
-0.4
-0.2
0
0.2
0.4
0.6
0.8
1

ANTARES

ANTARES

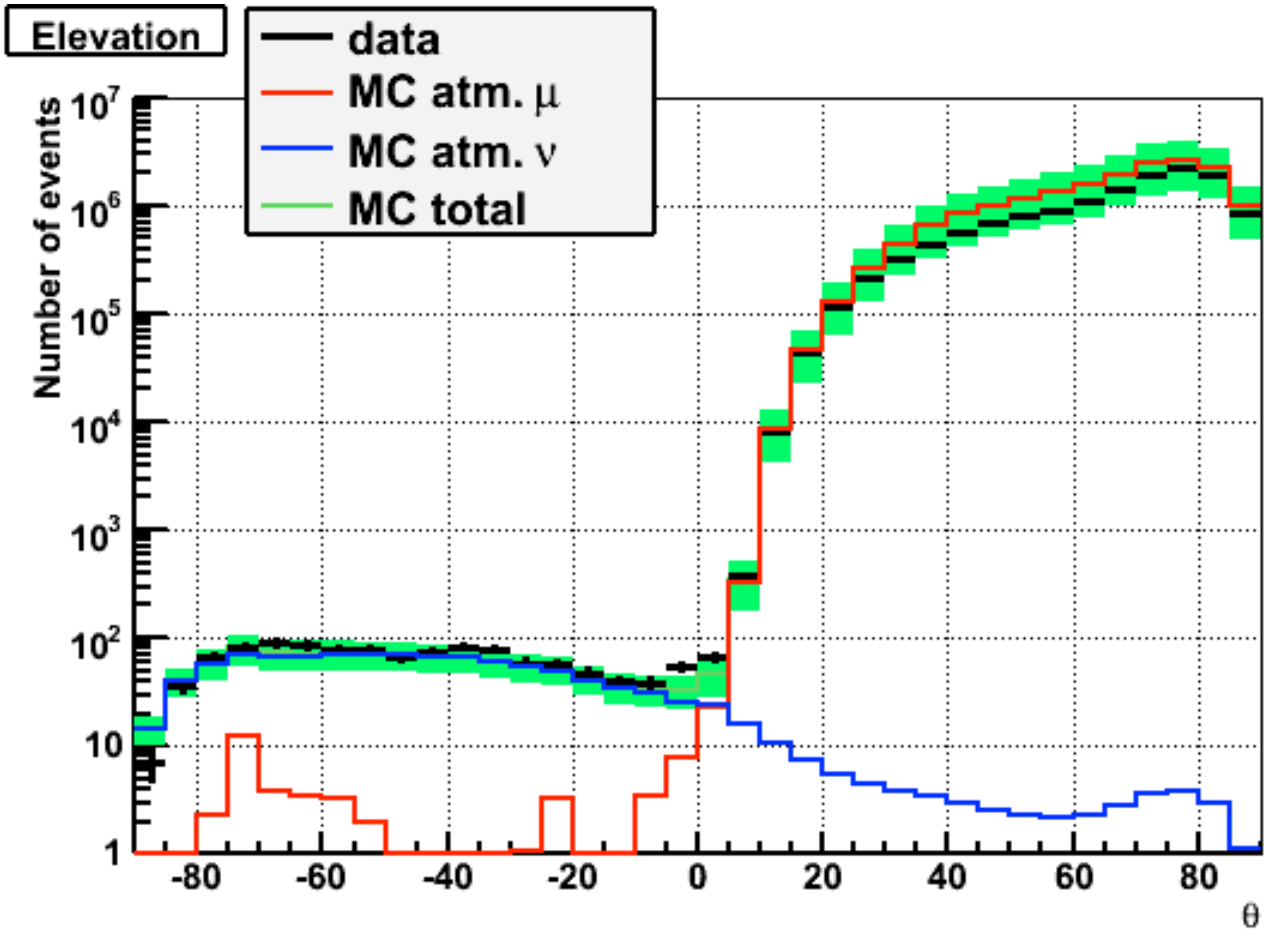
Elevation
data
MC atm. μ
MC atm. ν
MC total
Number of events
10^7
10^6
10^5
10^4
10^3
10^2
10
1
-80
-60
-40
-20
0
20
40
60
80
θ

ANTARES

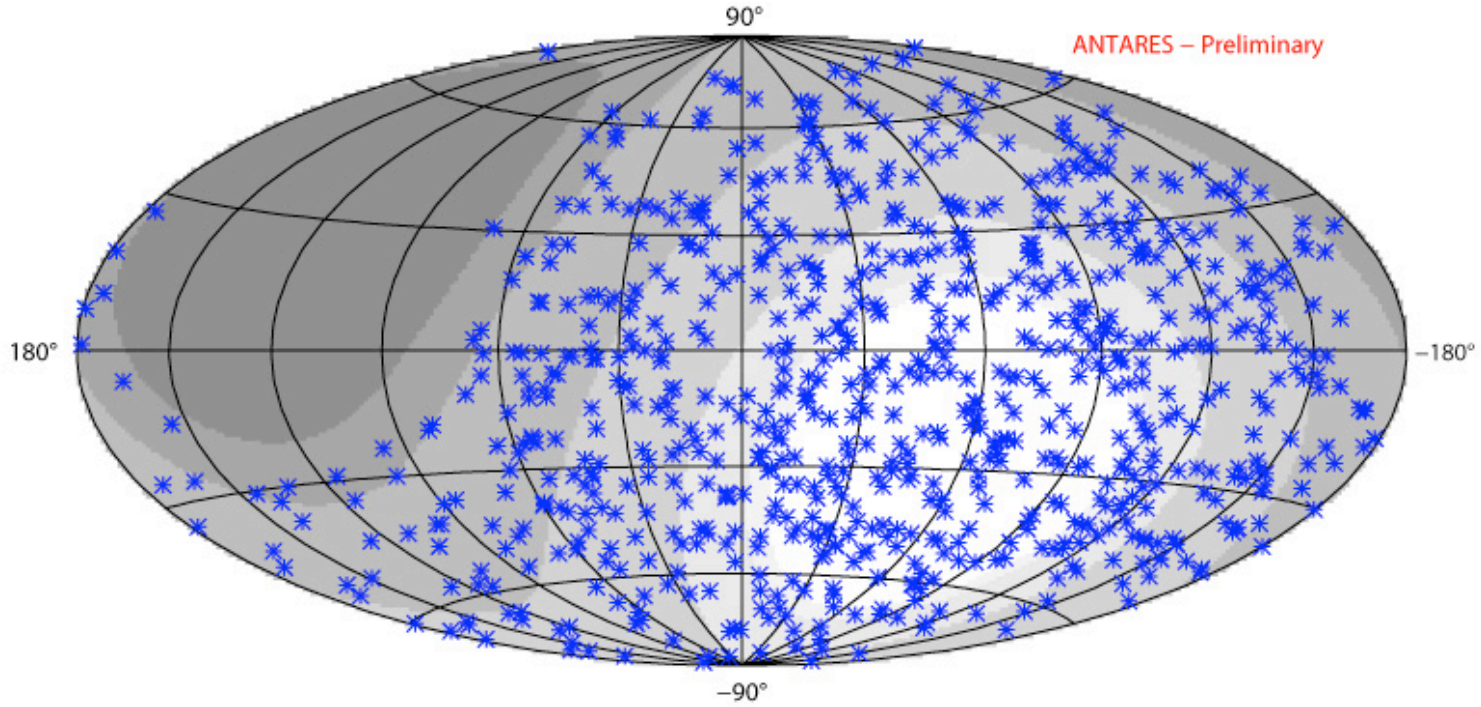

First sky view with the data taken by the ANTARES telescope. The grey background is correlated to the field of view of the detector : the darker the region, the lower the visibility; the white region is always observable. The centre of the map corresponds to the Galactic Centre.

IceCube Detector

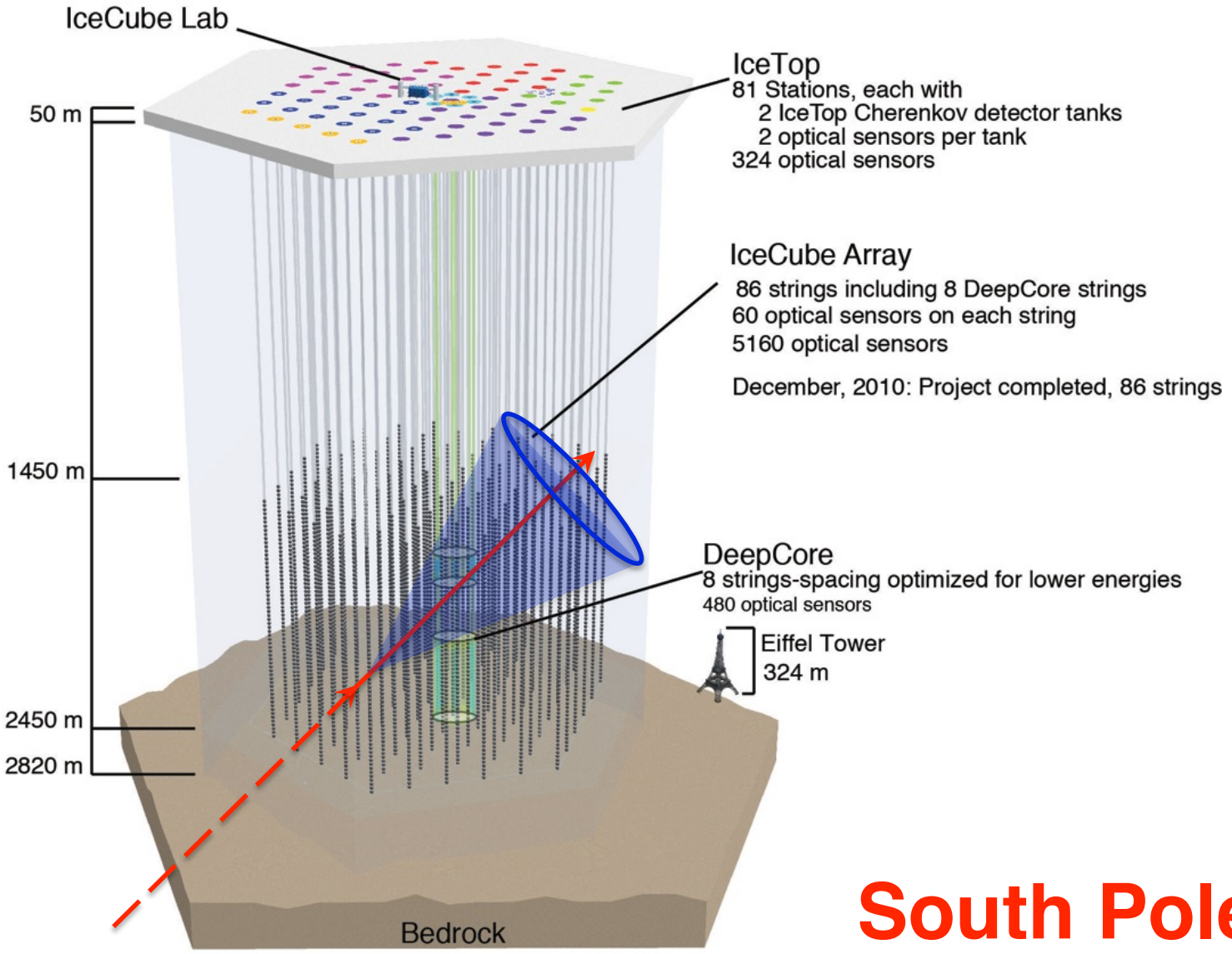

South Pole

Neutrinos and cosmic rays are detected using Cherenkov emission in ice sheet

IceCube - South Pole

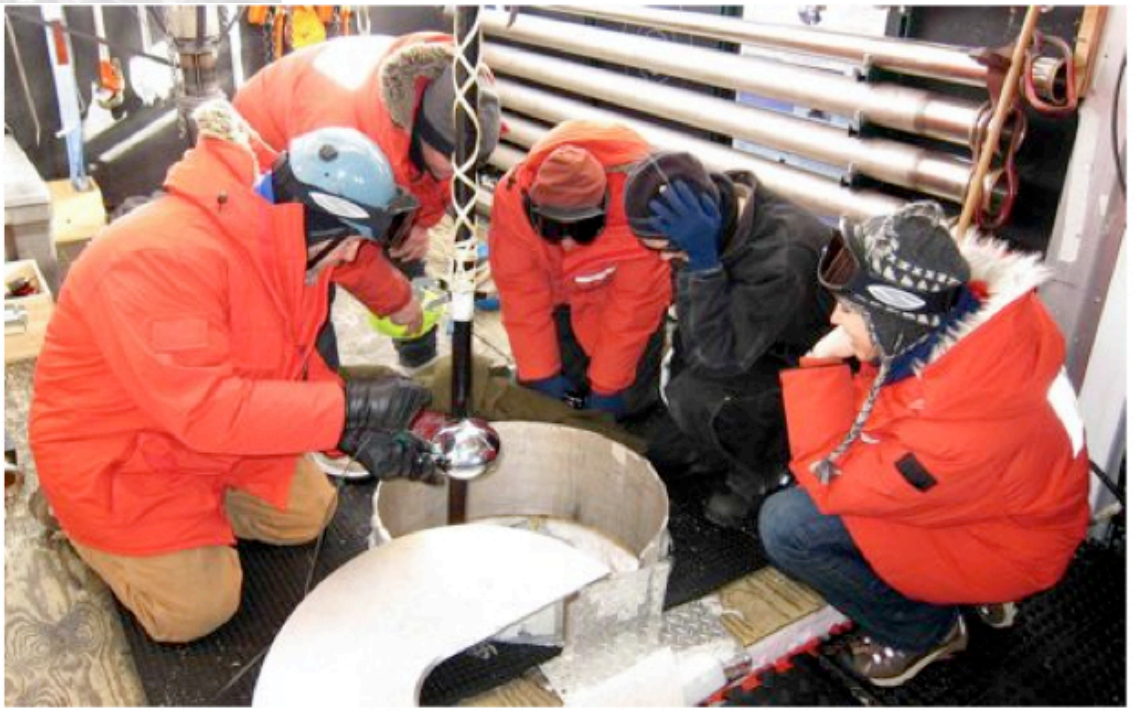

IceCube - South Pole

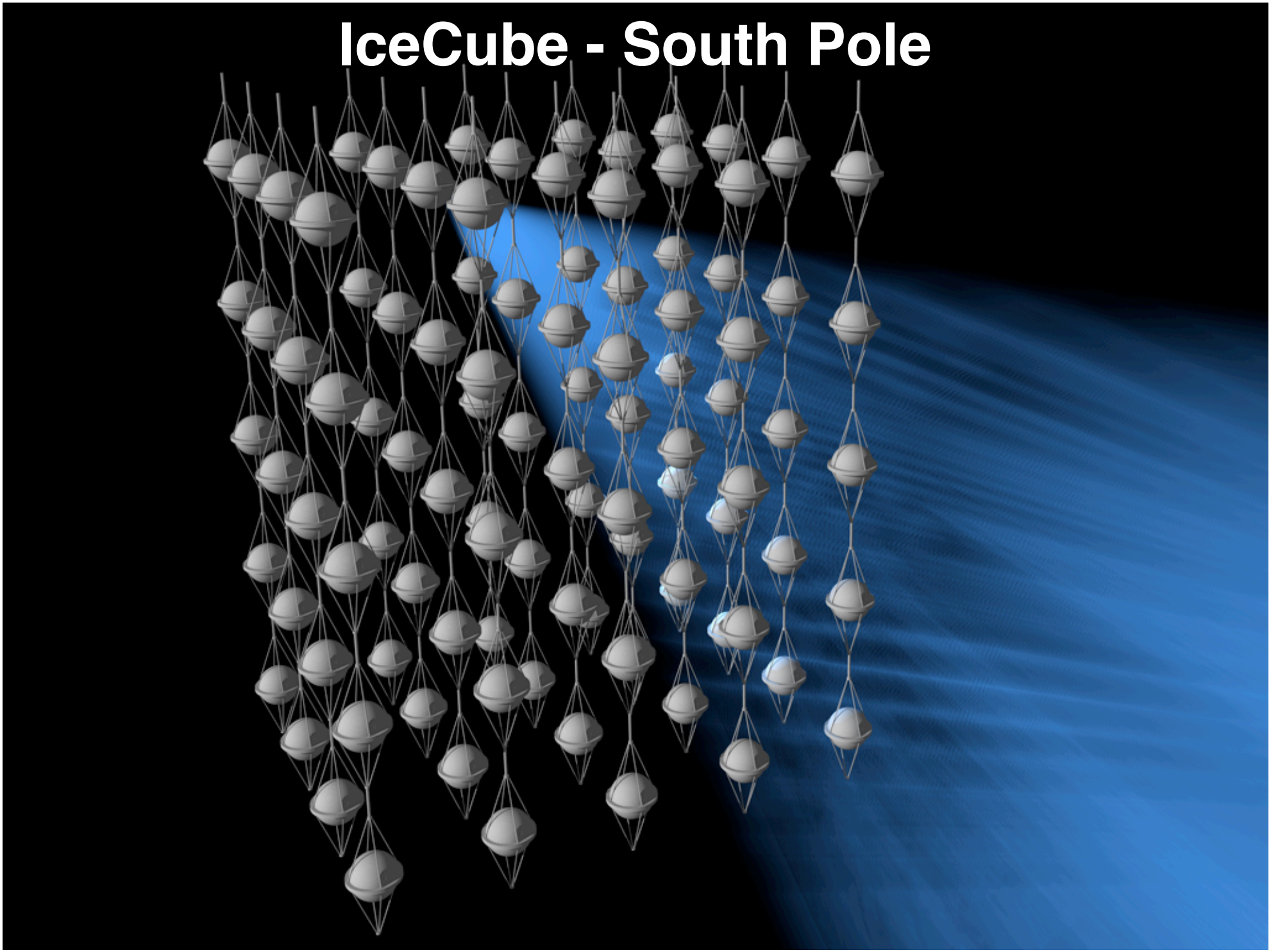

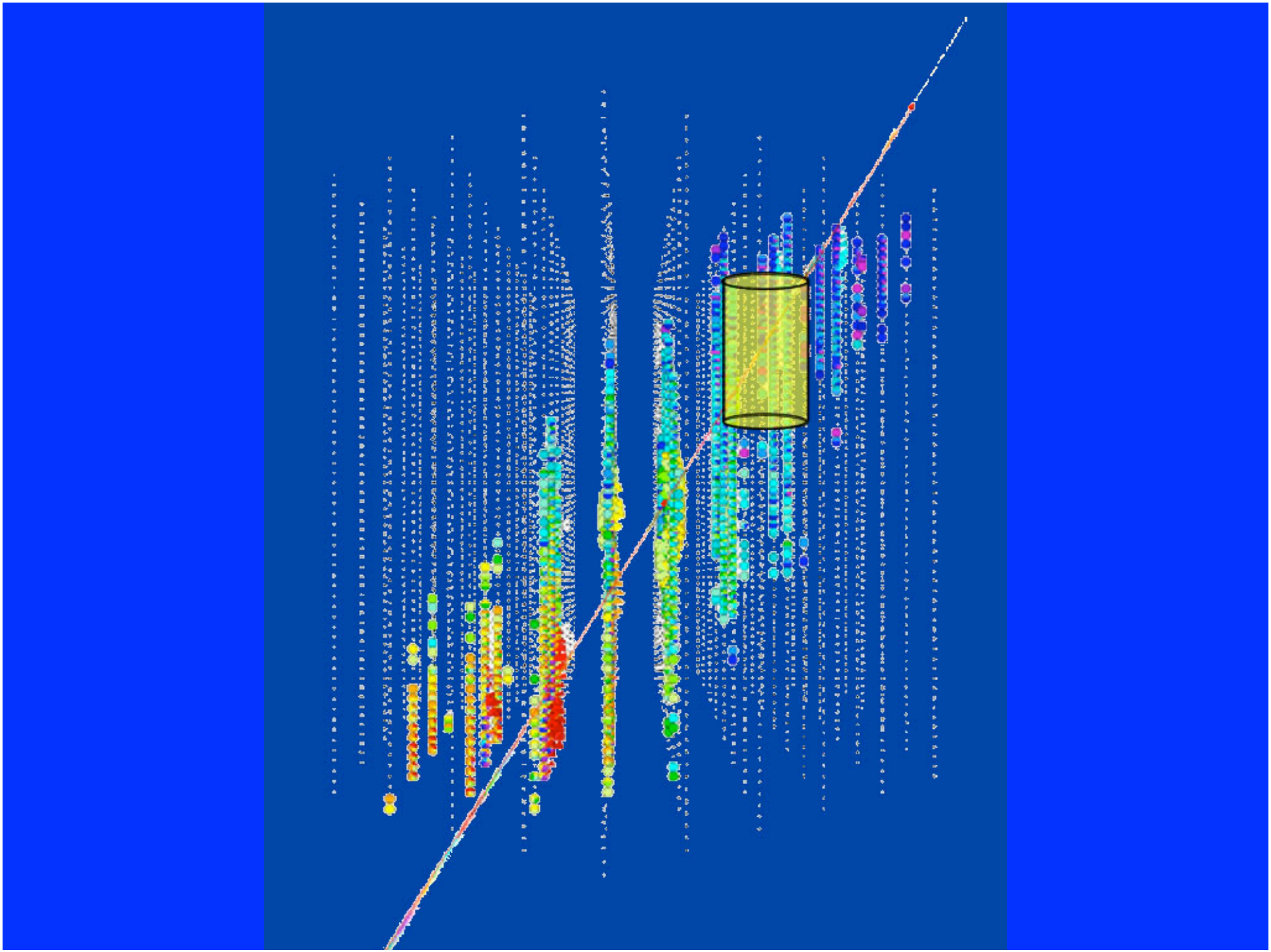

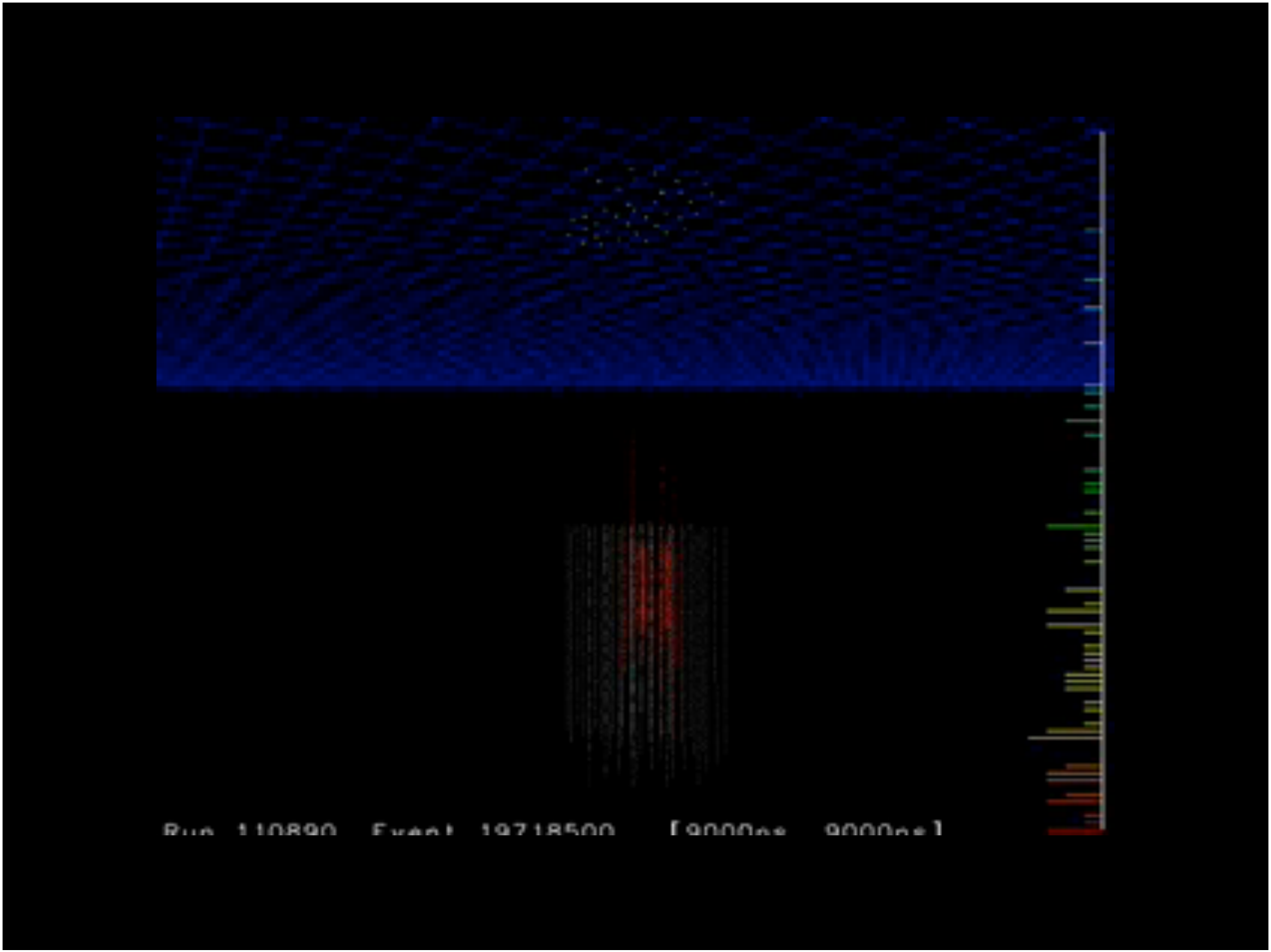
Run 110890 Event 19718500 [9000ns 9000ns]

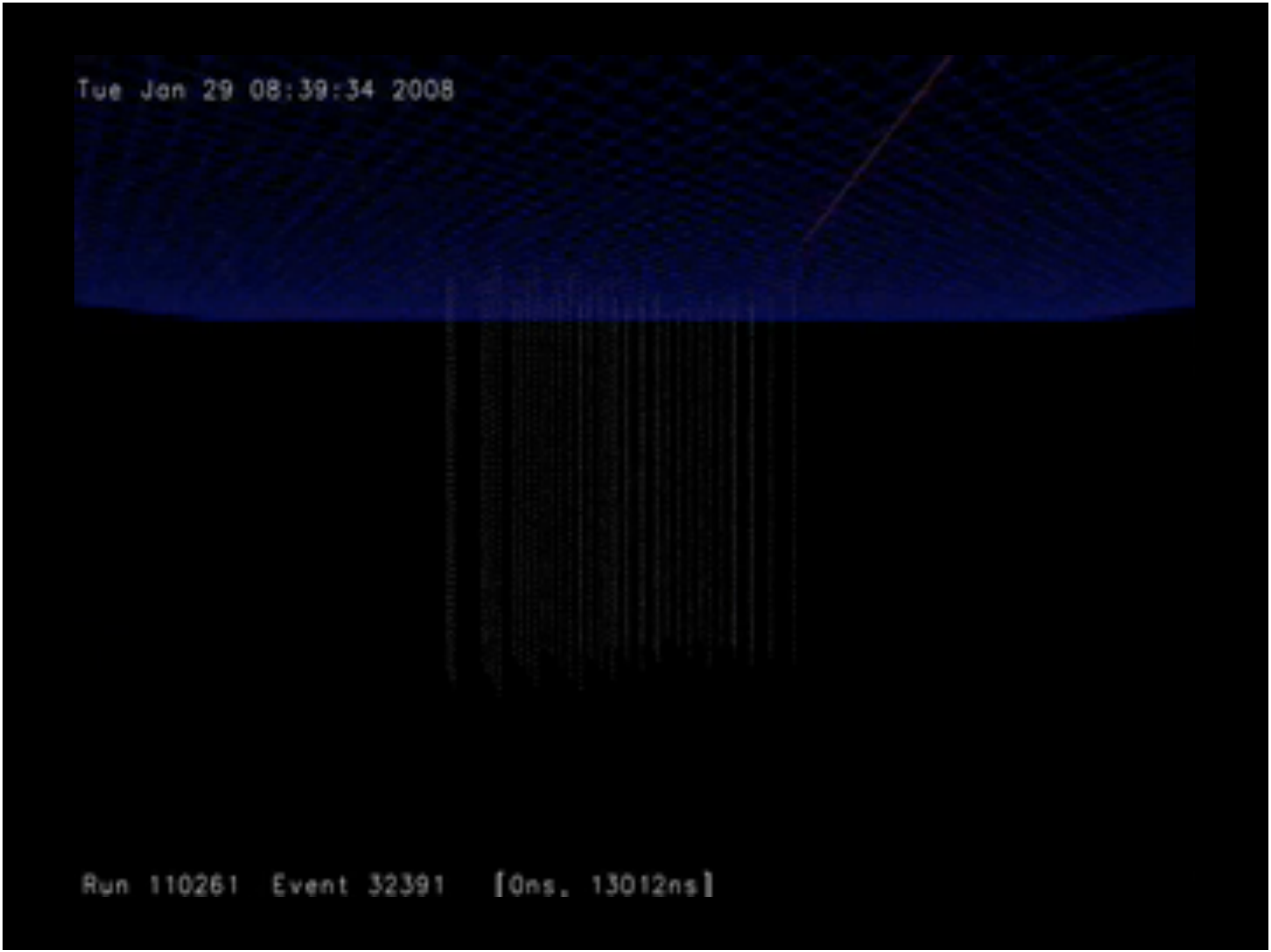
Tue Jan 29 08:39:34 2008
Run 110261 Event 32391 [0ns, 13012ns]

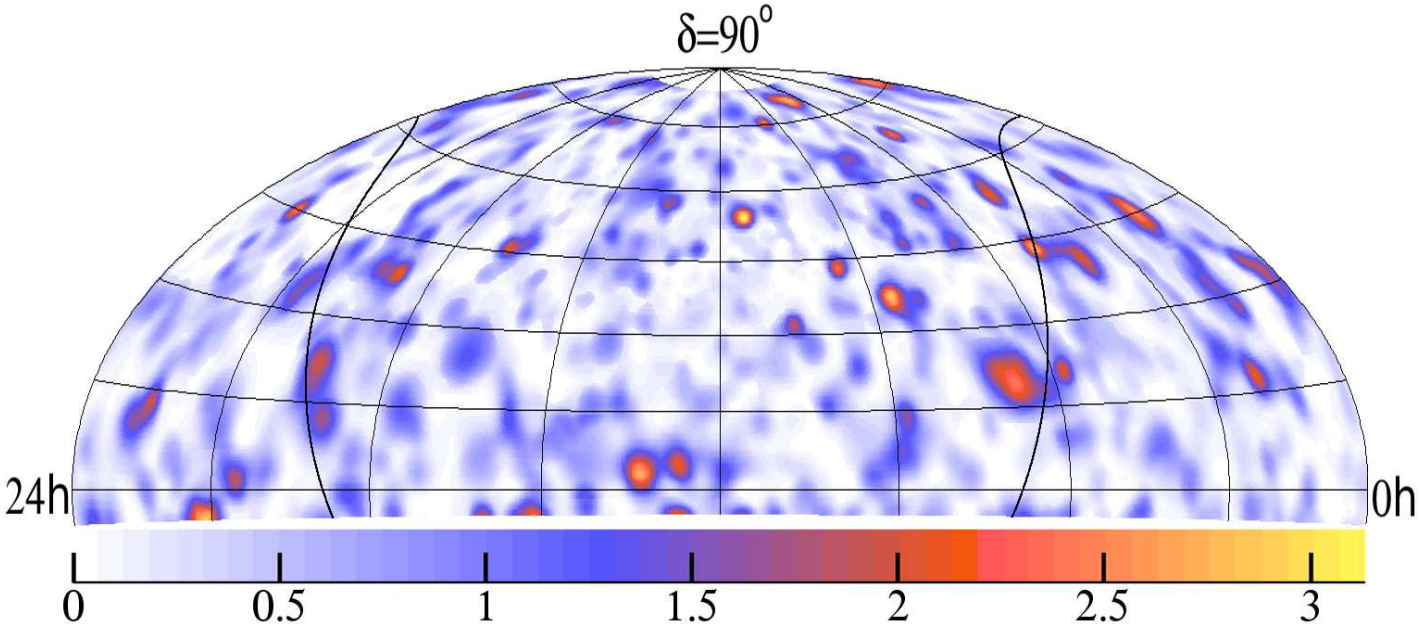

Fig. 3. Map of the pre-trials significances (in σ) obtained from an unbinned point source search using the full AMANDA-II data set. The most significant point has a significance of 3.38σ; 95% of randomized background skymaps include a point at least as significant.

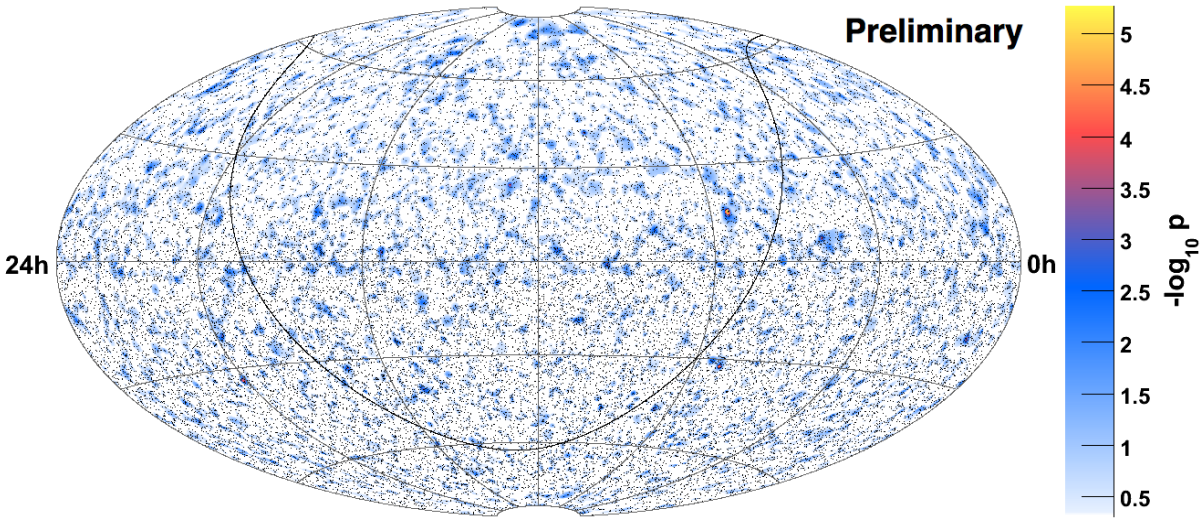

Figure 1. Skymap for the IceCube detector in the 40 string configuration for one year of data taken during 2008.

Muon energy reconstruction and atmospheric neutrino spectrum unfolding with the ANTARES detector

#541
Palioselitis

Correlation between reconstructed muon energy and true neutrino energy (from Monte Carlo)

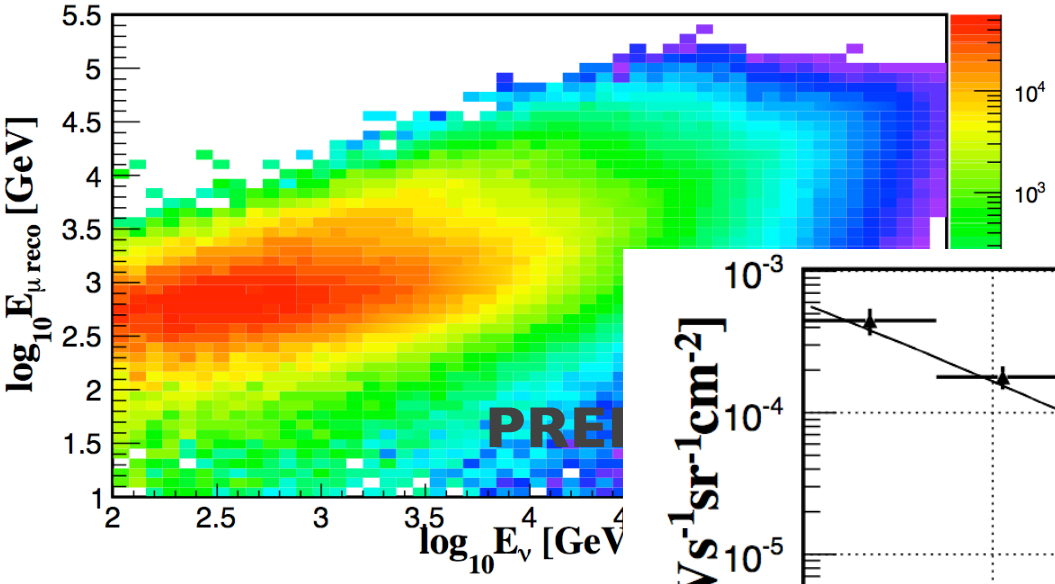

Atmospheric neutrino energy spectrum

SYSTEMATICS UNDER STUDY NOT INCLUDED HERE

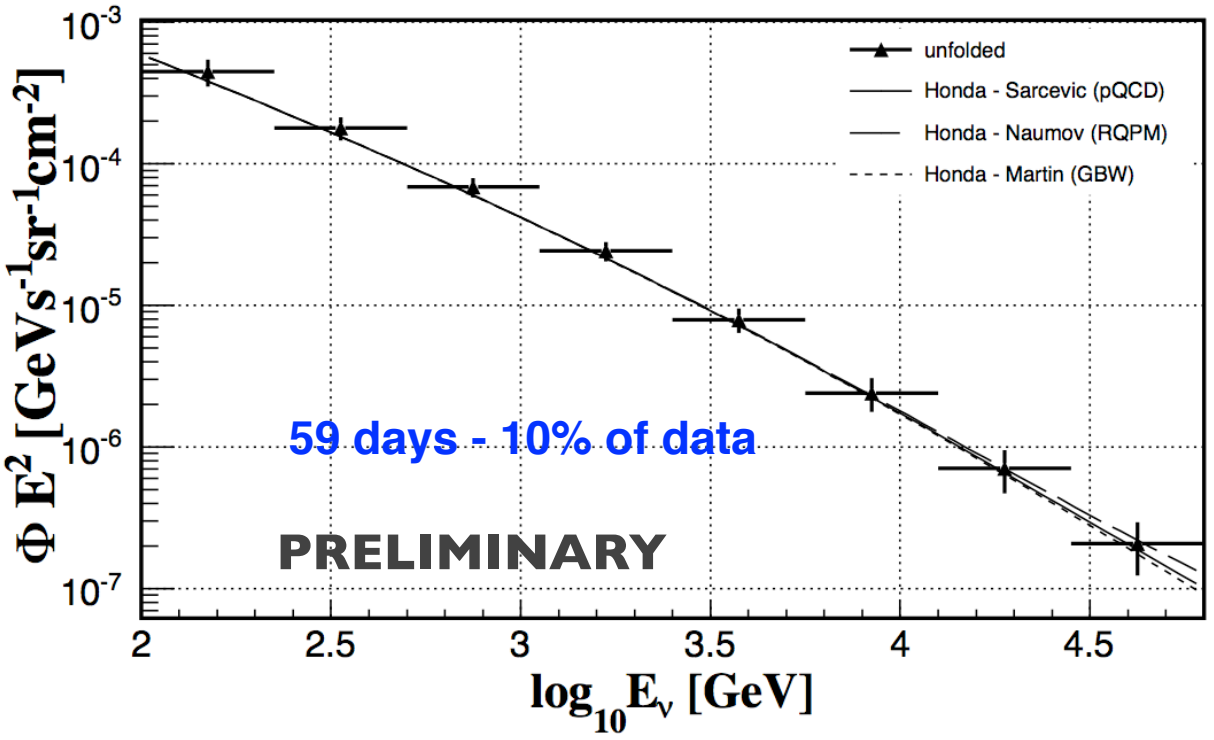

Search for a diffuse flux of high-energy muon neutrinos with the ANTARES neutrino telescope

#237
Schüssler

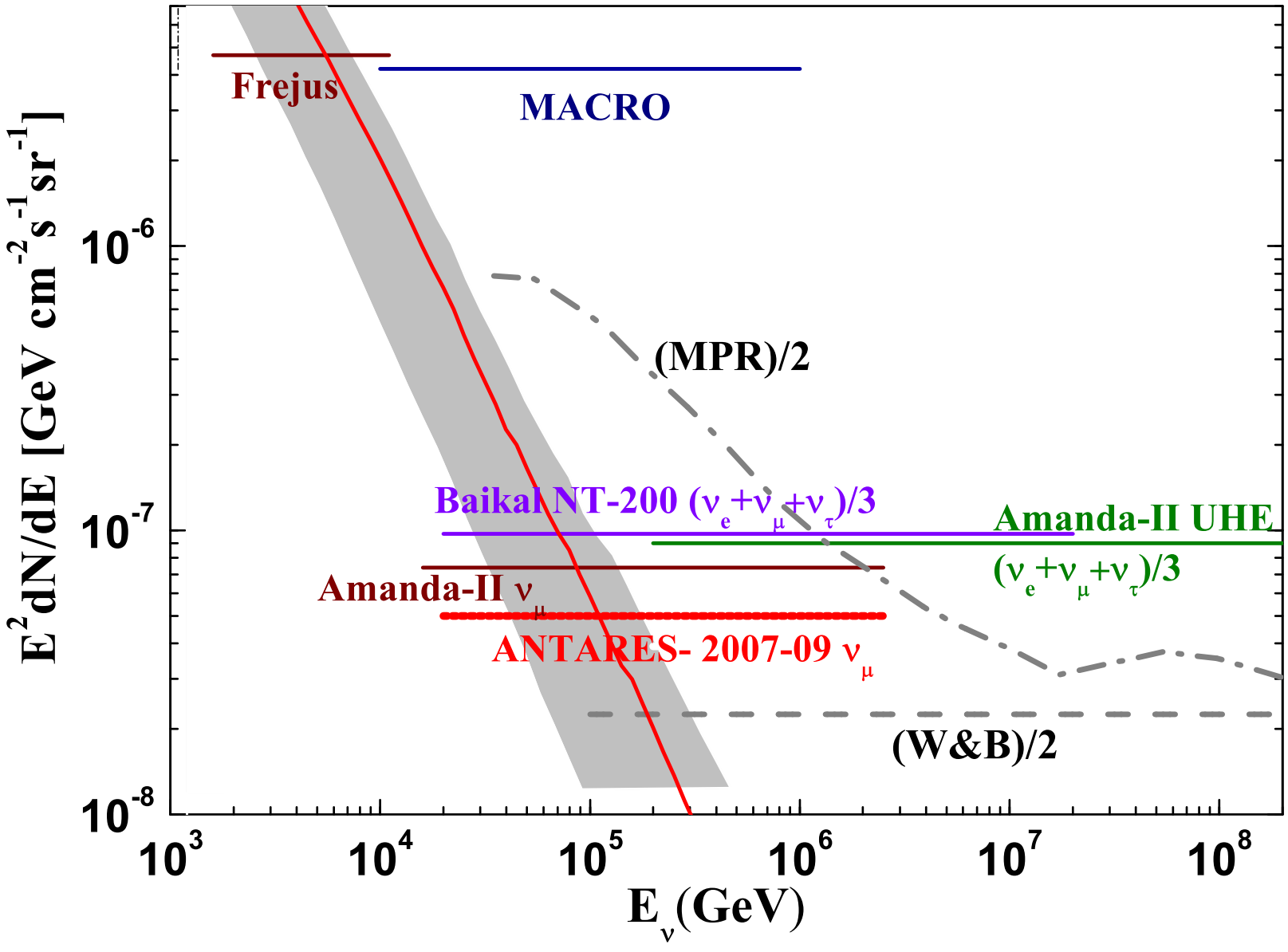

Search for a diffuse flux of astrophysical muon neutrinos with the IceCube detector

#736
Schukraft

Results and Sensitivity

RWTH AACHEN ICECUBE

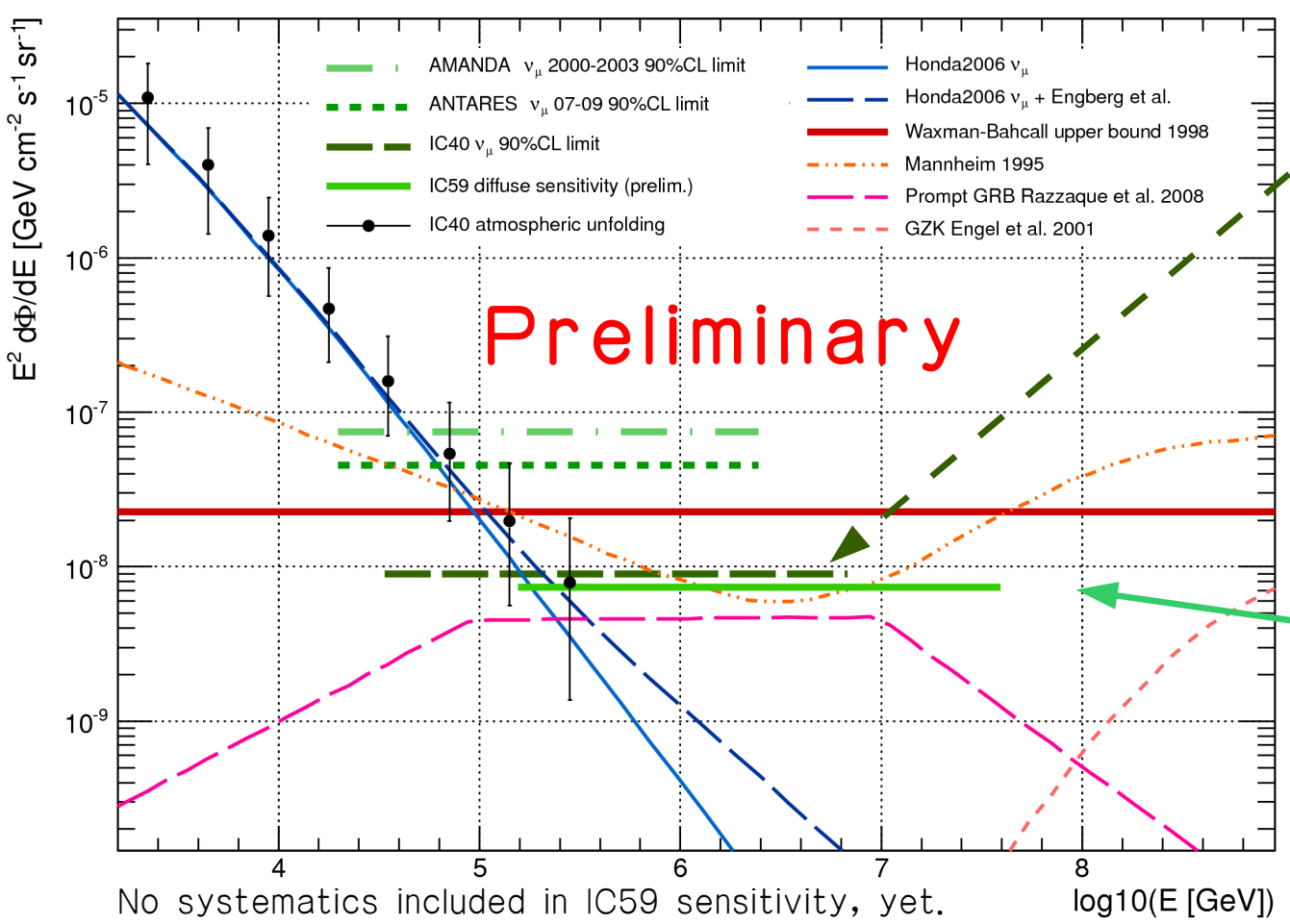

IC40 result

90%CL upper limit at

$8.9 * 10^{-9}$ GeV^{-1} cm^{-2} s^{-1} sr^{-1}

Factor 2.5 below the WB upper bound

IC59 Prelim. sensitivity

$7.2 * 10^{-9}$ GeV^{-1} cm^{-2} s^{-1} sr^{-1} (without neutrino knee)

~ factor 3 below the WB upper bound

The Pierre Auger Observatory and ultra-high energy neutrinos

#682
Guardincerri

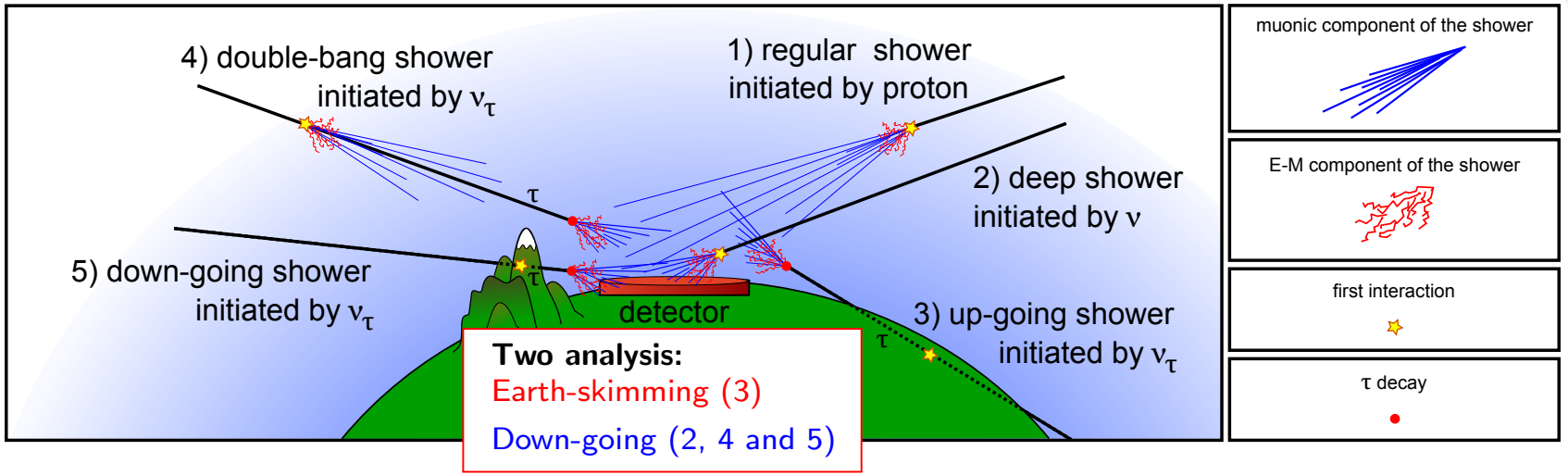

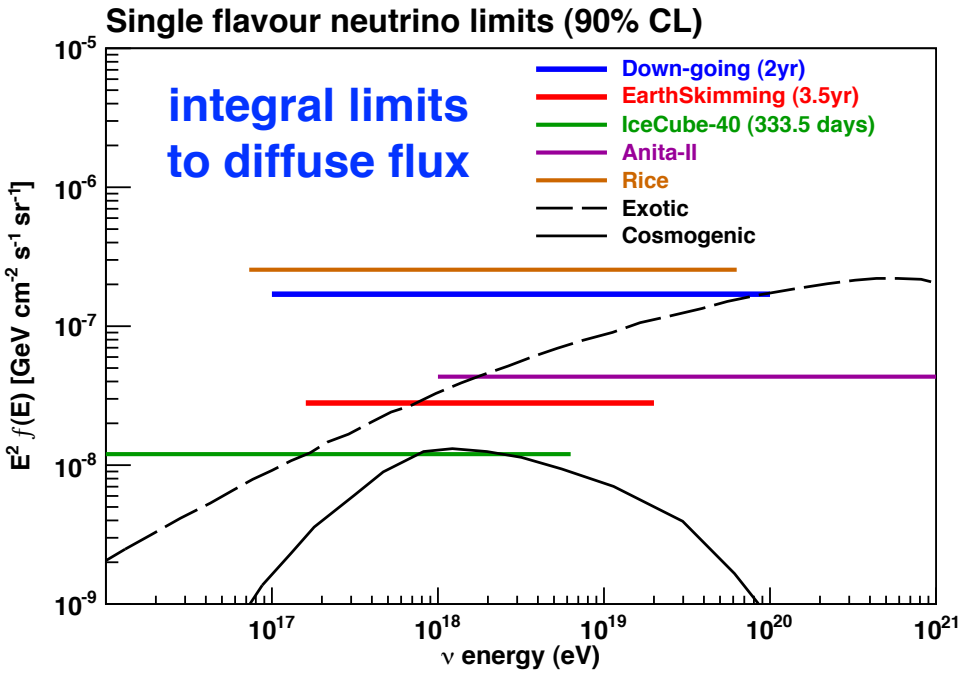

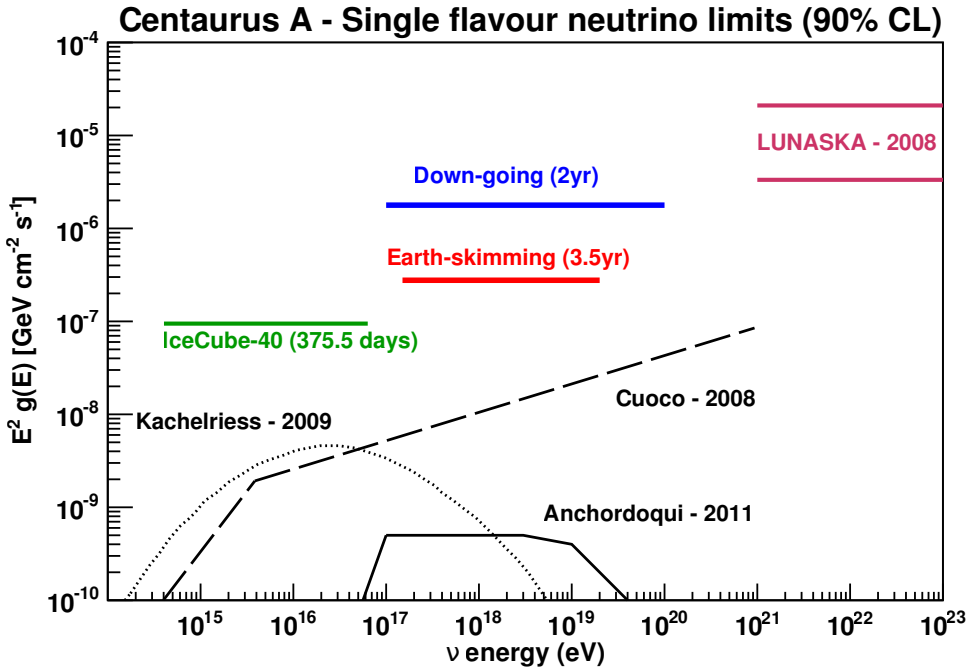

Searching for point sources of high-energy cosmic neutrinos with the ANTARES telescope

#295
Bogazzi

51 candidate sources

name	ra	decl	Nsigfit	Q	p-value	nsigma	lim_Nsig	lim_flux
HESS J1023-575	155.83	-57.76	1.97	2.35	0.41	0.82	5.62	6.6e-08
3C 279	-165.95							
GX 339-4	-104.30							
Cir X-1	-129.83							

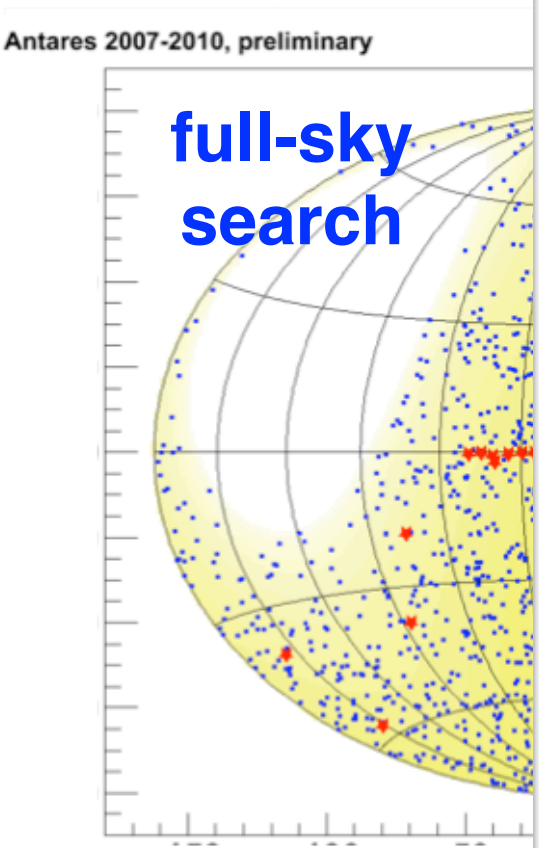

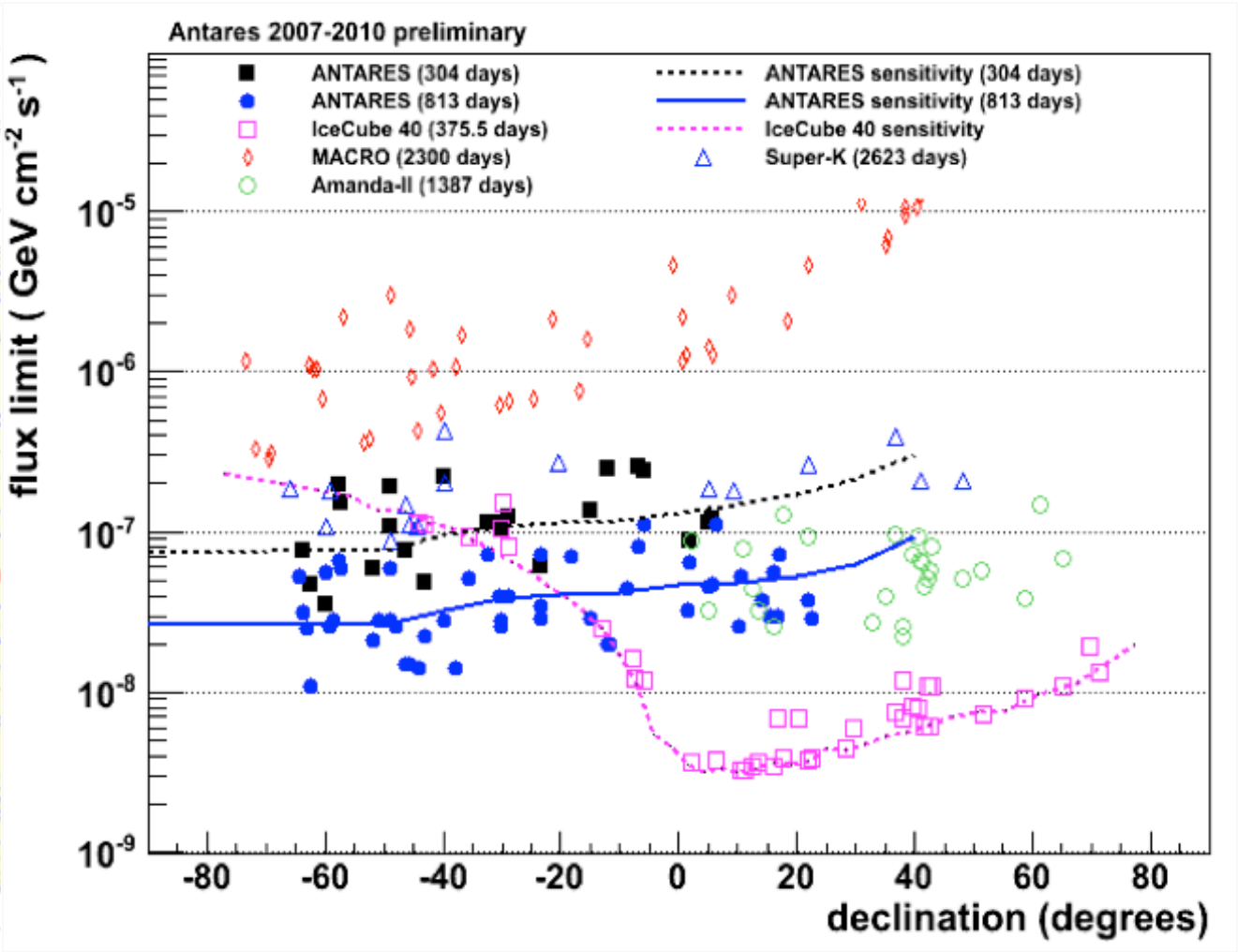

Search for neutrino emission of gamma-ray flaring blazars with the ANTARES telescope

#91 Dornic

search for correlations with 10 very bright and variable Fermi LAT blazars

Source	visibility	timePDF (MJD+54000)	Live time (day)	N(5σ)	Nobs	Fluence U.L. GeV/cm^2
0208-512	1.0	712-5, 722-4, 745-7, 750-2, 753-7, 764-74, 820-2	8.8	4.5	0	2.8
0235+164	0.41	710-33, 738-43, 746-64, 766-74, 785-7, 805-8, 810-2	24.5	4.3	0	18.7
1510-089	0.55	716-9, 720-5, 726-35, 788-90, 801-3	4.9	3.8	0	2.8
3C273	0.49	714-6, 716-8, 742-5	2.4	2.5	0	1.1

3C279
1 neutrino compatible with time/space distribution
probability 10% after trails

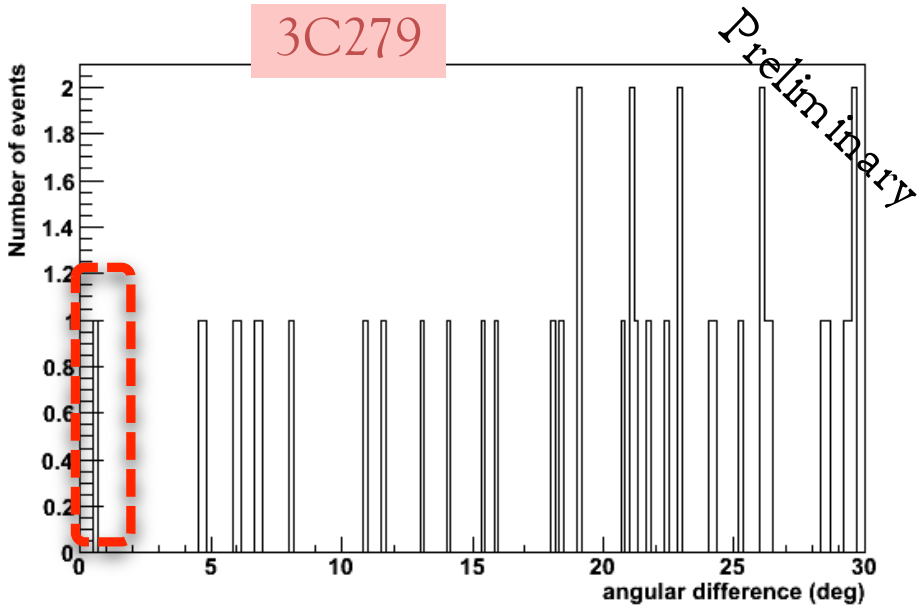

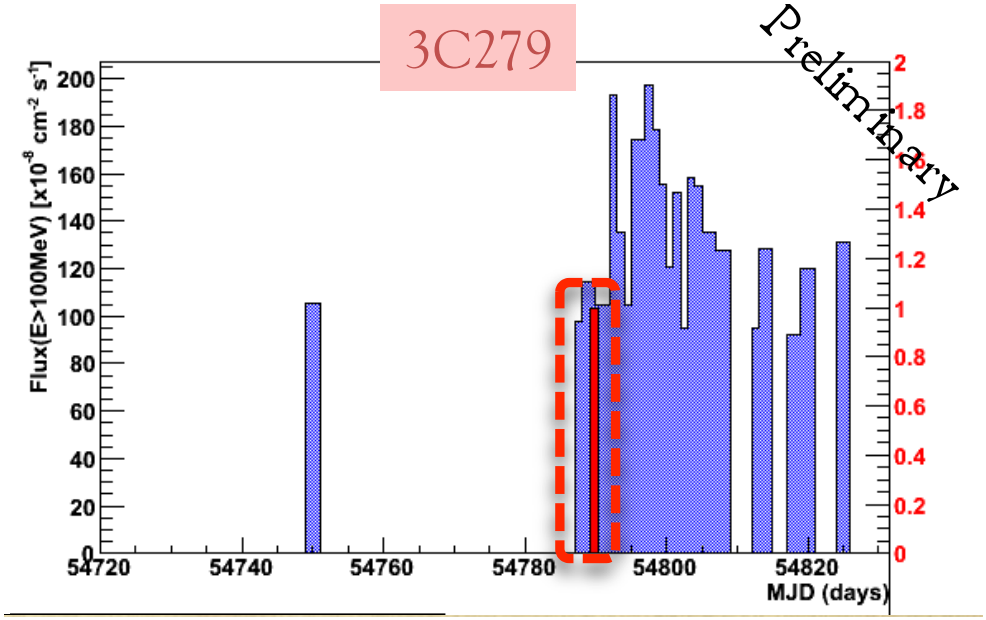

Atmospheric neutrinos in a wide energy range

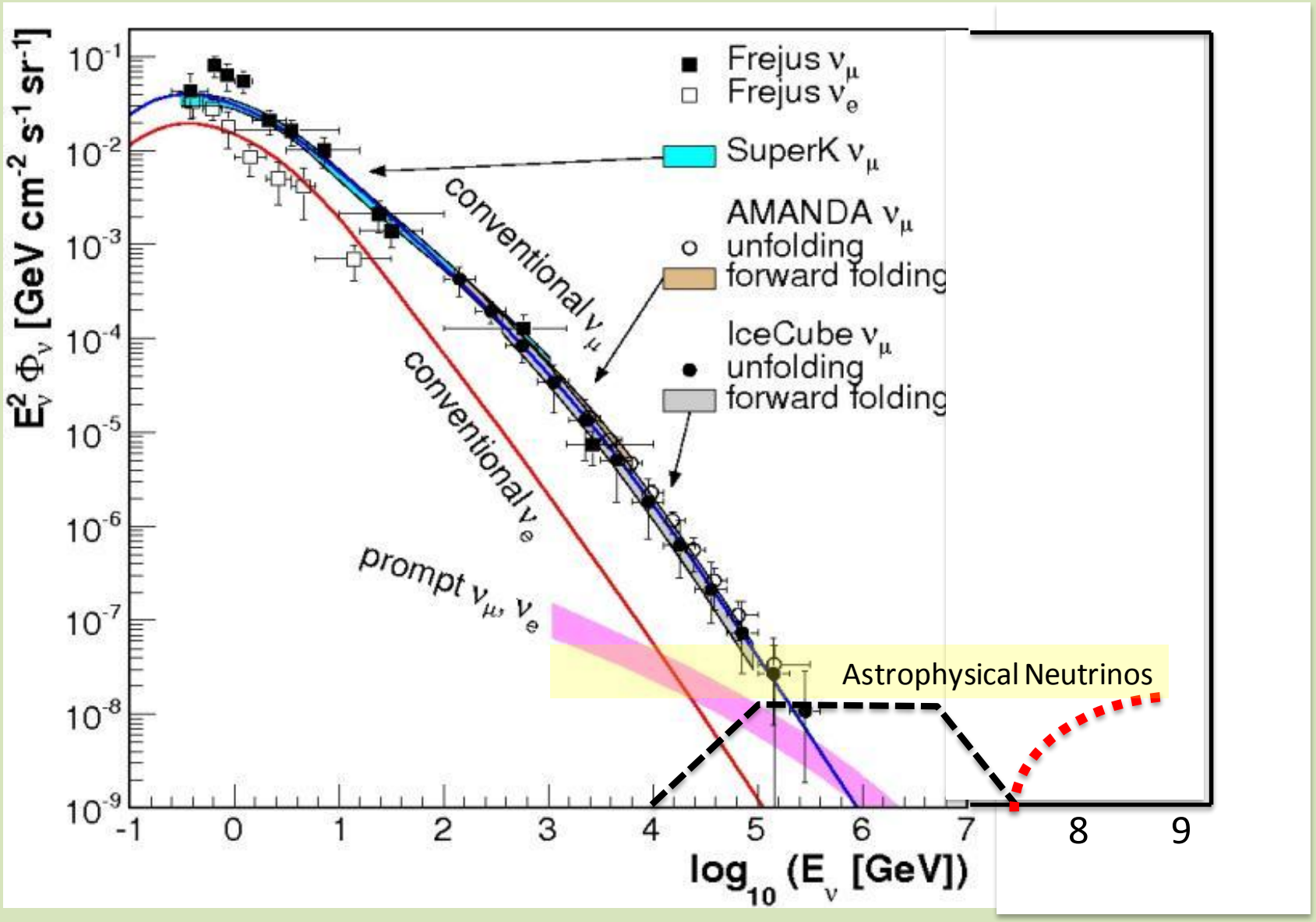

A. Ishihara, IceCube (2012)

After unblind - Observation of 2 events

Run119316-Event36556705
NPE 9.628×10^4
GMT time: 2012/1/3 9:34:01

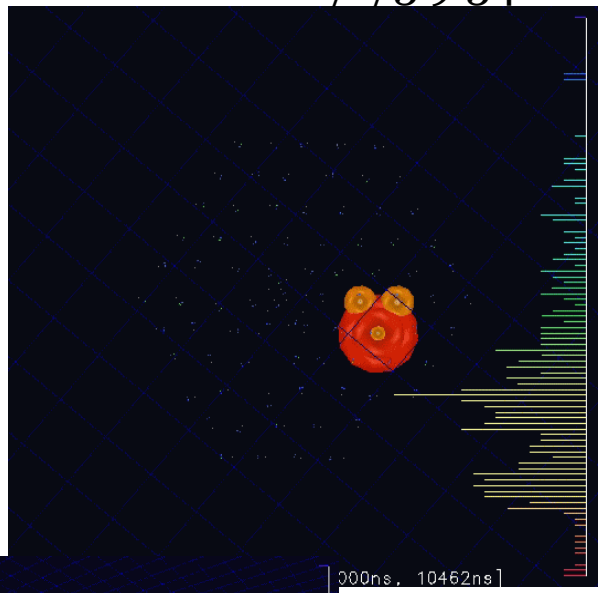

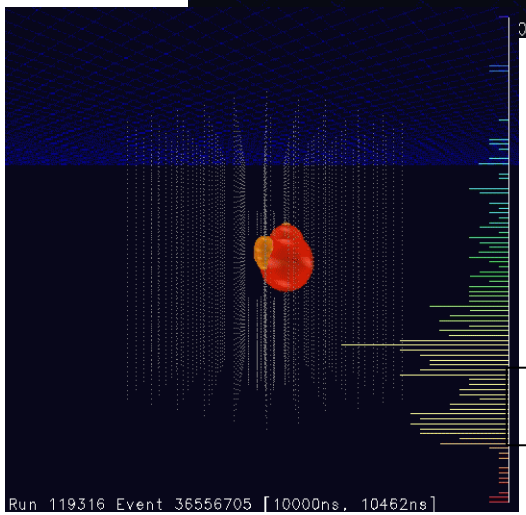

2 events / 670 days
background (atm. μ + conventional atm. ν)
expectation 0.057 events
Preliminary

p-value 1.581×10^{-4} (2.95σ)

Aya Ishihara

Run118545-Event6373366
NPE 6.9928×10^4
GMT time: 2012/8/8 12:23:18

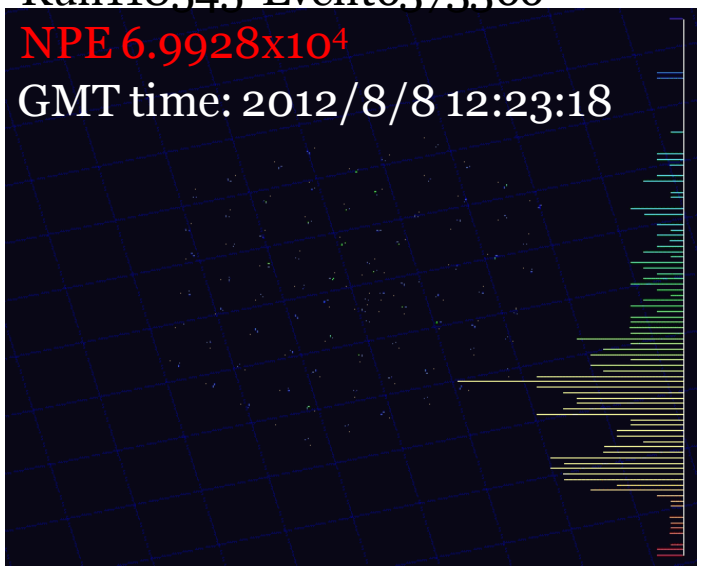

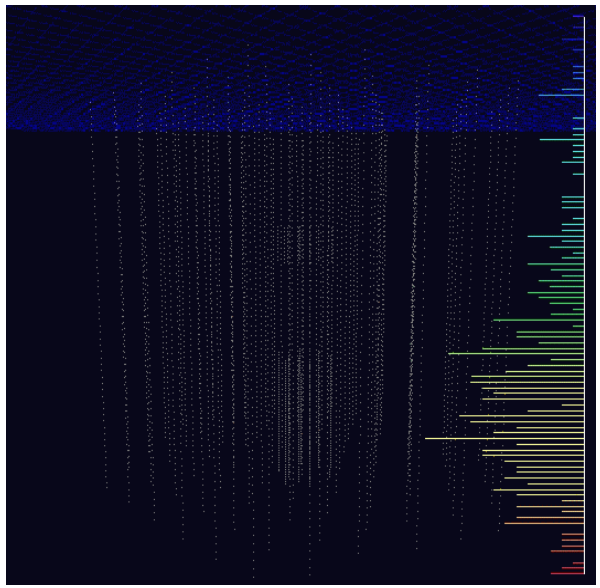

A. Ishihara, IceCube (2012)

Consistent with cascade events in detector

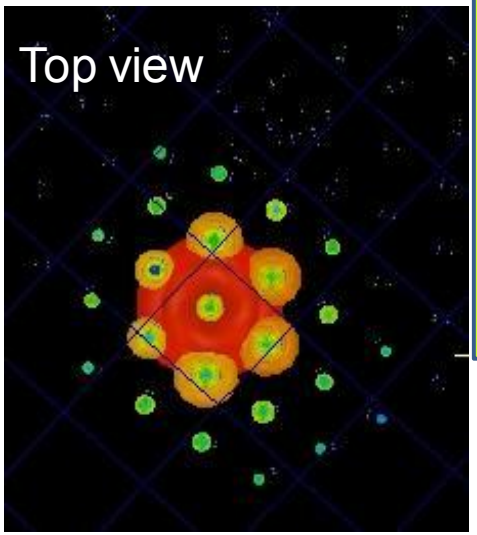

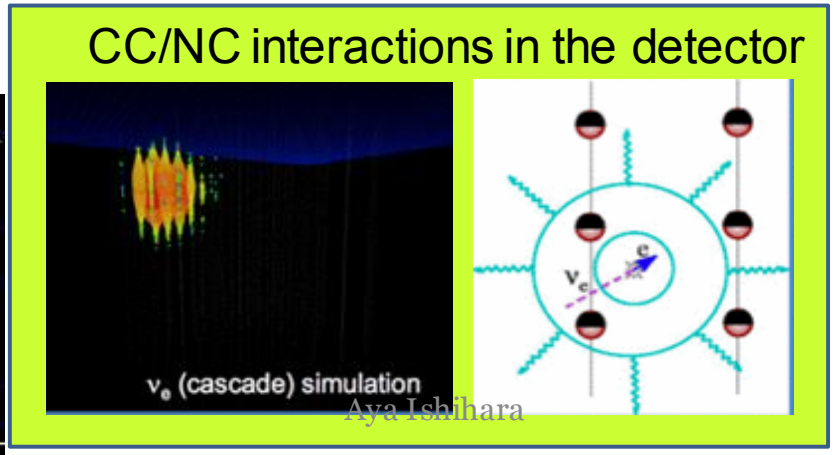

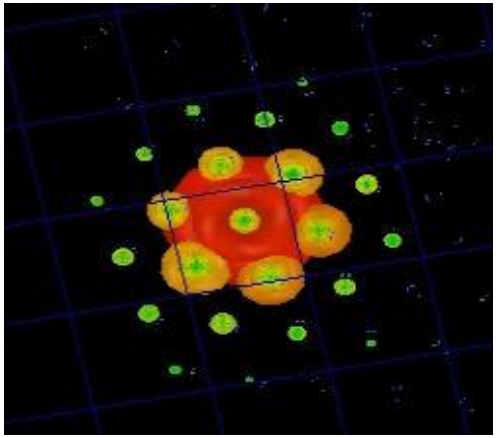

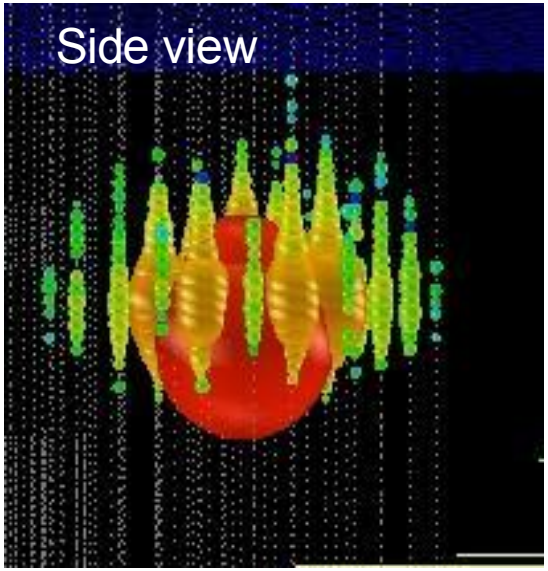

No indication
that they are instrumental artifacts
that they are cosmic-ray muon induced

we can use **dedicated cascade hypothesis** to the reconstructions of these special events
Many students/posdocs contributed

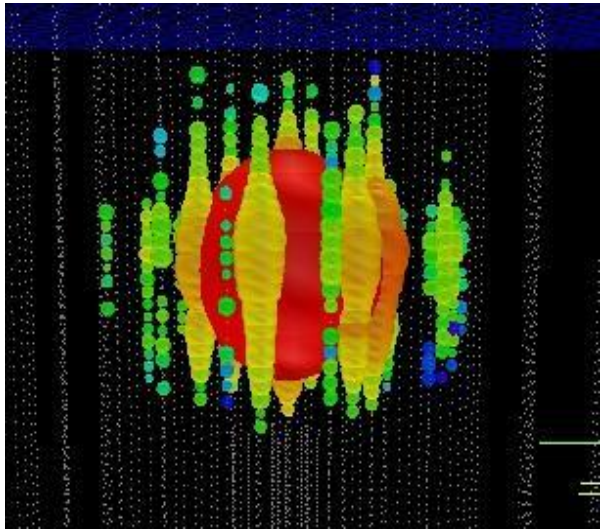

A. Ishihara, IceCube (2012)

What are their energies and directions?

- Maximizing the Poisson likelihood based on the recorded waveforms
  - Charges and timing information

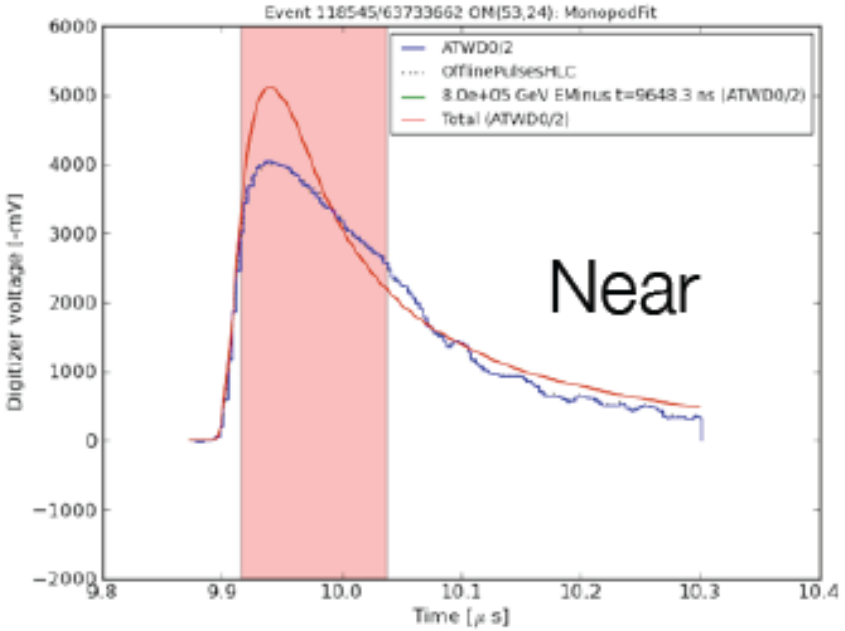

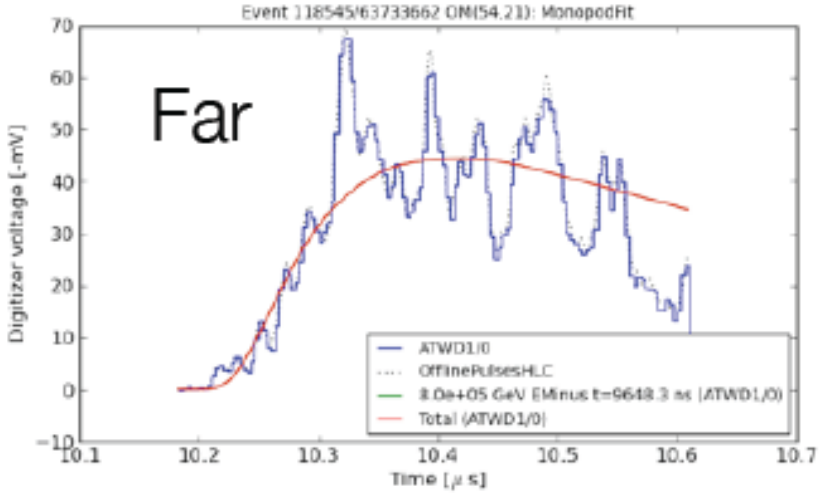

Estimated Energy Deposit

Preliminary

- Jan 2012 event 1.3 PeV
- Aug 2011 event 1.14 PeV

zenith 17deg

zenith 79deg

Downward-going PeV showers

A. Ishihara, IceCube (2012)

Numbers of UHE Events

Preliminary

Models	IceCube 2008-2009 Phys. Rev D83 092003 (2011) 333days	IceCube 2010-2012 per 670days		
		$E^{detector} < 10^8$ GeV and interaction in detector (A)	All contributions (B)	(B) - (A)
Background (conv. atm. ν + atm. μ)	**0.11**		**0.14**	
Experimental data	***0***	***2***	***2***	***0***
GZK (Yoshida m=4)*	**0.57**	**0.4**	**2.1**	**1.7**
GZK (Ahlers max) **	**0.89**	**0.5**	**3.2**	**2.7**
GZK (Ahlers best fit) **	**0.43**	**0.3**	**1.6**	**1.3**
GZK (Kotera, dip FRII) ***		**1.7**	**4.1**	**2.4**
GZK (Kotera, dip SFR1)***		**0.6**	**1.0**	**0.4**

*Yoshida et al The ApJ 479 547-559 (1997), **Ahlers et al, Astropart. Phys. 34 106-115 (2010), ***Kotera et al, ^R. Enberg, M.H. Reno, and I. Sarcevic, Phys. Rev. D 78, 043005 (2008), ^^ Talk G. Sullivan This conference

A. Ishihara, IceCube (2012)

IceCube UHE Sensitivity 2010-2012

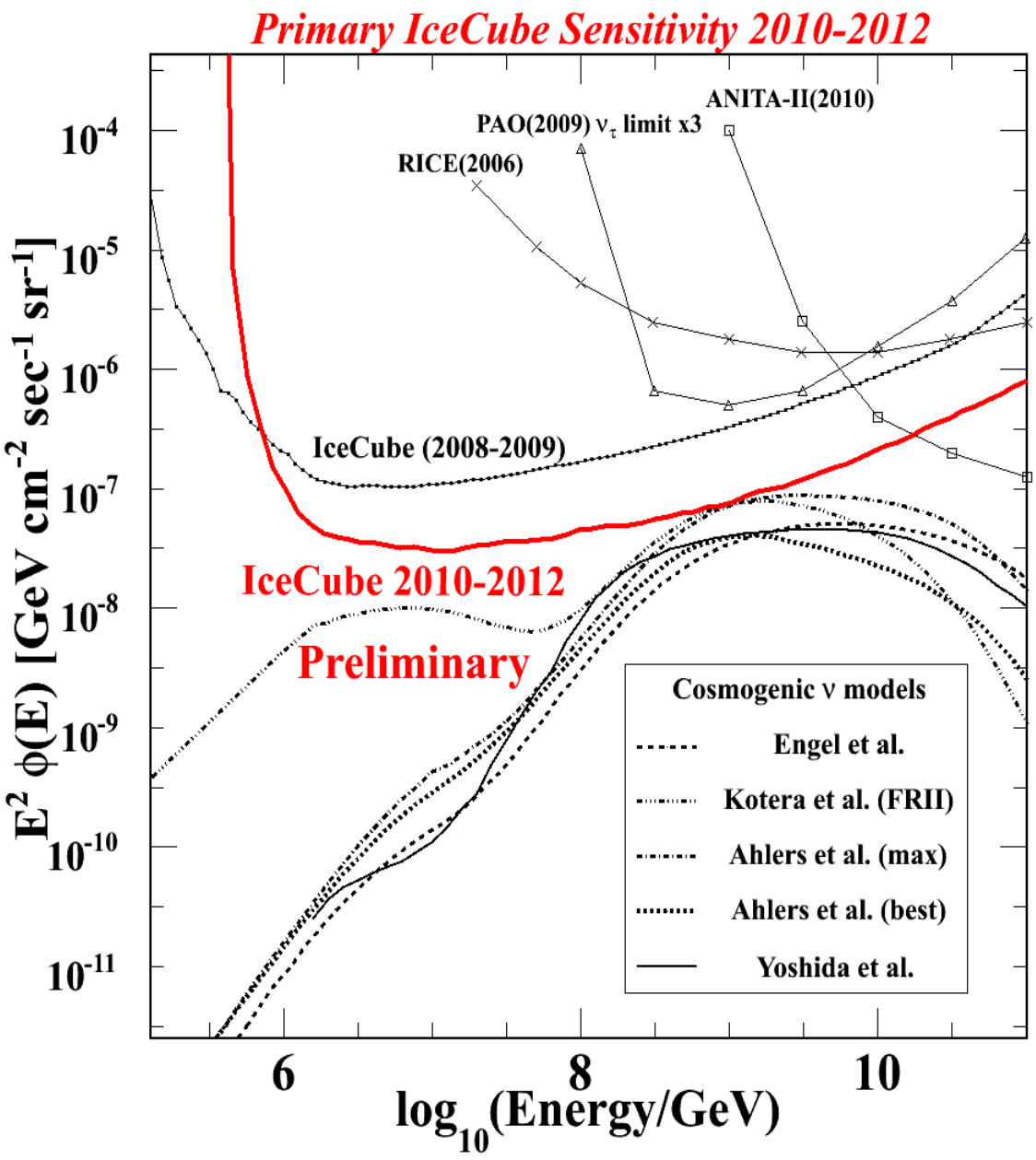

- A factor of ~4 improved from the previous IceCube results
- The world's best sensitivity!
- Will constrain the neutrino fluxes down to mid-strong cosmological evolution models

65

A. Ishihara, IceCube (2012)

Summary

- Searched for neutrinos with PeV and greater energies in nearly full 2 years of the IceCube data
- Two candidate events observed
  - PeV to 10PeV energy cascade-channel neutrino events (CC/NC interactions within the detector)
  - The highest energy neutrino events observed ever!
- Beyond the conventional atmospheric neutrinos
- Any post-unblinding analysis indicates higher significance (but not official)
- Hints for the PeV events origin from different energy-region
  - More cascade event sensitive analysis
  - Lower energy regions for the spectral transition
  - more statistics

  will answer some of questions in relatively short time

A. Ishihara, IceCube (2012)

On The Origin of IceCube's PeV Neutrinos

Ilias Cholis[1] and Dan Hooper[1,2]

[1] *Fermi National Accelerator Laboratory, Theoretical Astrophysics Group*
[2] *University of Chicago, Department of Astronomy and Astrophysics*

The IceCube collaboration has recently reported the observation of two events with energies in excess of 1 PeV. While an atmospheric origin of these events cannot be ruled out at this time, this pair of showers may potentially represent the first observation of high-energy astrophysical neutrinos. In this paper, we argue that if these events are neutrino-induced, then the neutrinos are very likely to have been produced via photo-meson interactions taking place in the same class of astrophysical objects that are responsible for the acceleration of the $\sim 10^{17}$ eV cosmic ray spectrum. Among the proposed sources of such cosmic rays, gamma-ray bursts stand out as particularly capable of generating PeV neutrinos at the level implied by IceCube's two events. In contrast, the radiation fields in typical active galactic nuclei models are likely dominated by lower energy (UV) photons, and thus feature higher energy thresholds for pion production, leading to neutrino spectra which peak at EeV rather than PeV energies (models with significant densities of x-ray emission, however, could evade this problem). Cosmogenic neutrinos generated from the propagation of ultra-high energy cosmic rays similarly peak at energies that are much higher than those of the events reported by IceCube.

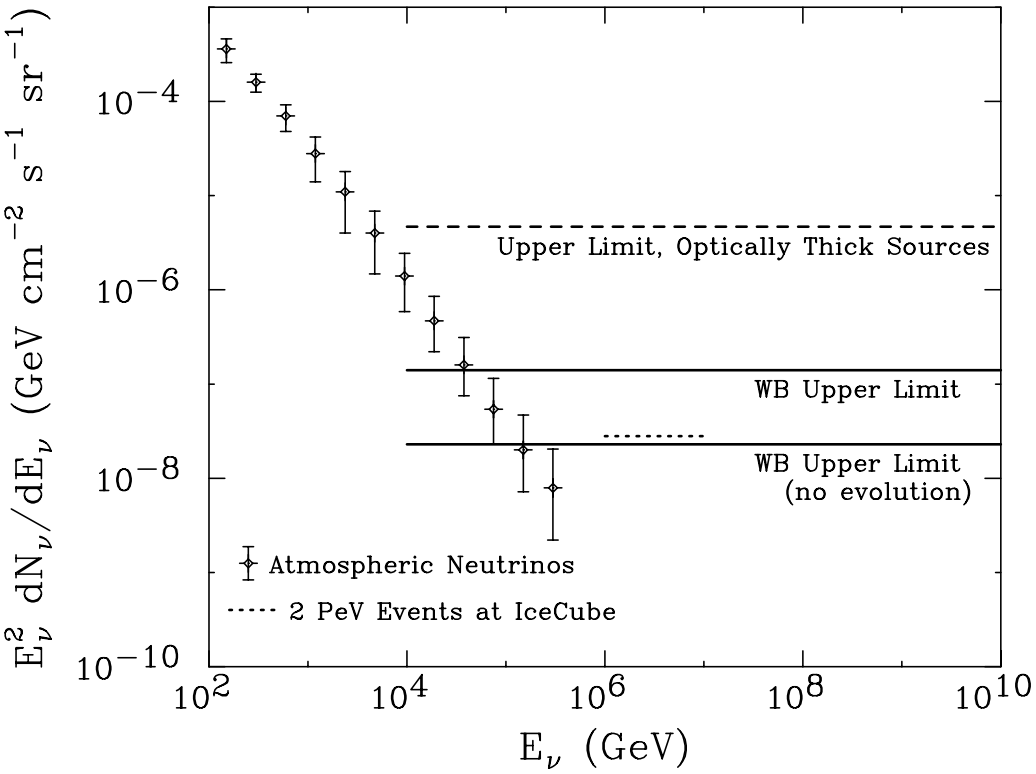

arXiv:1211.1974

Science 22 November 2013:
Vol. 342 no. 6161
DOI: 10.1126/science.1242856

RESEARCH ARTICLE

Evidence for High-Energy Extraterrestrial Neutrinos at the IceCube Detector

IceCube Collaboration*

* Full author list after Acknowledgments.

ABSTRACT | STRUCTURED ABSTRACT | EDITOR'S SUMMARY

We report on results of an all-sky search for high-energy neutrino events interacting within the IceCube neutrino detector conducted between May 2010 and May 2012. The search follows up on the previous detection of two PeV neutrino events, with improved sensitivity and extended energy coverage down to about 30 TeV. Twenty-six additional events were observed, substantially more than expected from atmospheric backgrounds. Combined, both searches reject a purely atmospheric origin for the 28 events at the 4σ level. These 28 events, which include the highest energy neutrinos ever observed, have flavors, directions, and energies inconsistent with those expected from the atmospheric muon and neutrino backgrounds. These properties are, however, consistent with generic predictions for an additional component of extraterrestrial origin.

Francis Halzen, IMAPP colloquium, January 20th, 2014

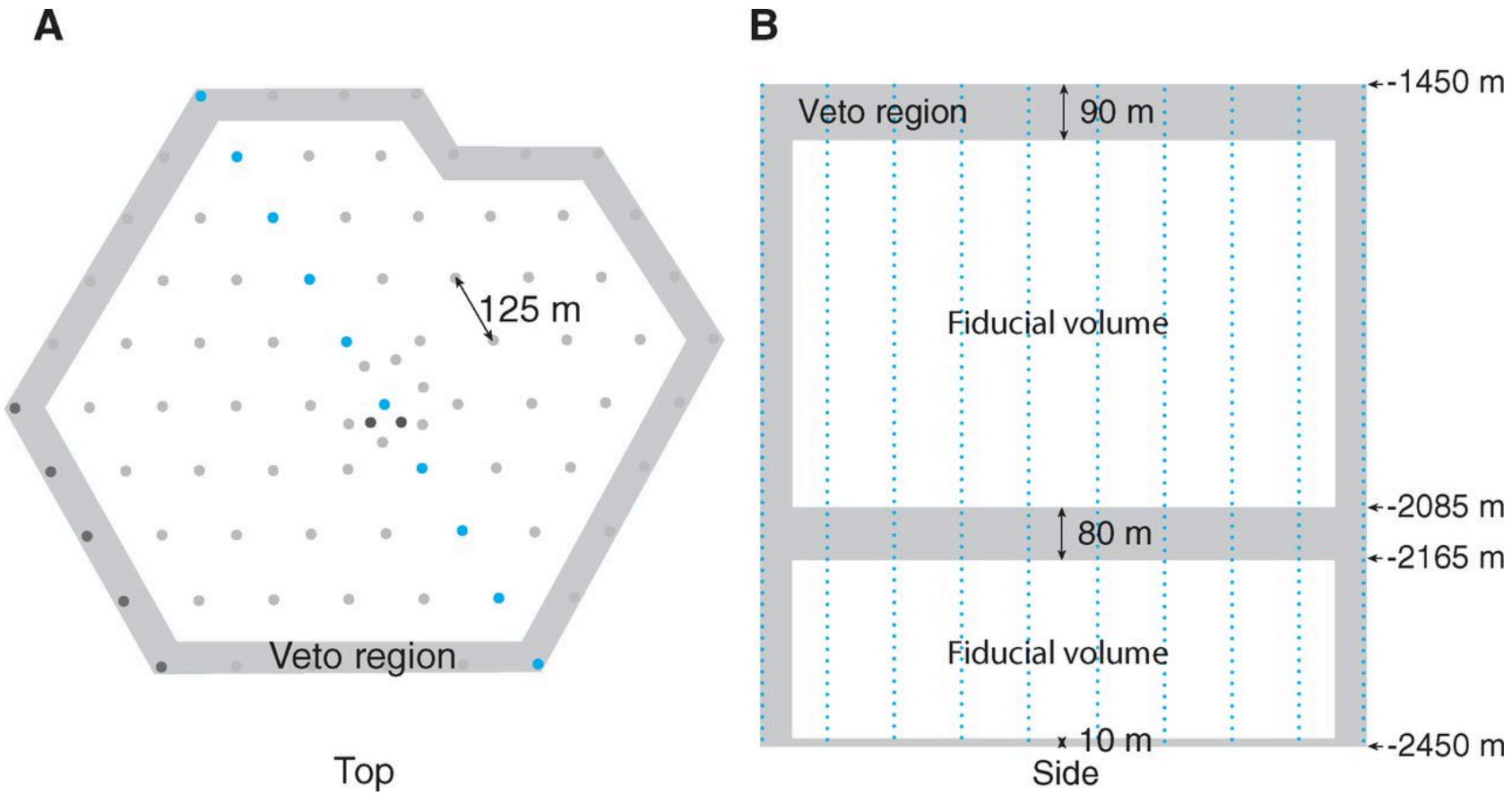

Fig. 1. Drawing of the IceCube array.

Results are from the complete pictured detector for 2011 to 2012 and from a partial detector missing the dark gray strings in the bottom left corner for the 2010 to 2011 season. (**A** and **B**) The side view (B) shows a cross section of the detector indicated in the top view (A) in blue. Events producing first light in the veto region (shaded area) were discarded as entering tracks (usually from cosmic ray muons entering the detector). Most background events are nearly vertical, requiring a thick veto cap at the top of the detector. The shaded region in the middle contains ice of high dust concentration (*24*). Because of the high degree of light absorption in this region, near horizontal events could have entered here without being tagged at the sides of the detector without a dedicated tagging region.

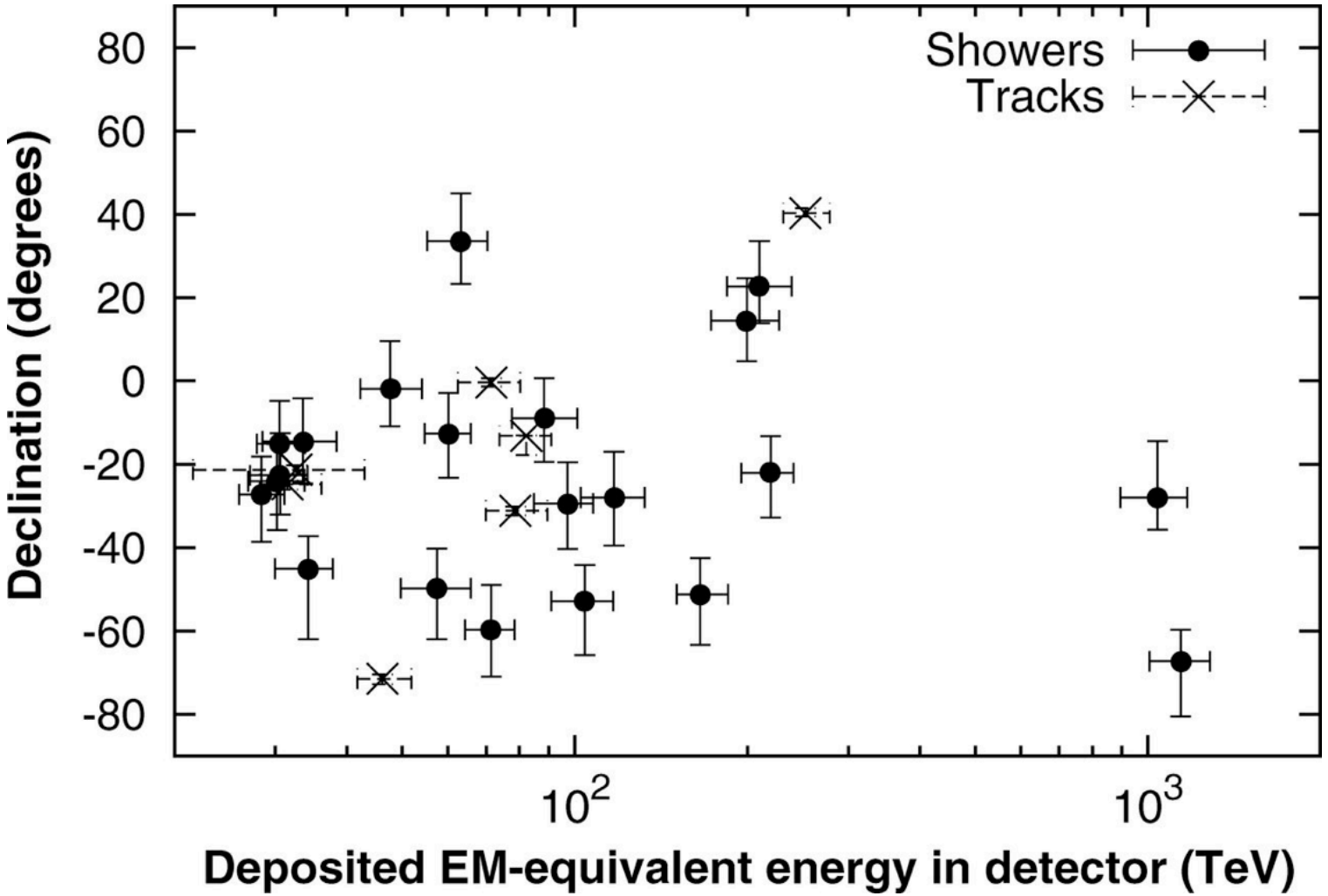

Fig. 2. Distribution of best-fit deposited energies and declinations.

Seven of the events contain muons (crosses) with an angular resolution of about 1°, whereas the remainder are either electromagnetic (EM) or hadronic showers (filled circles) with an energy-dependent resolution of about 15°. Error bars are 68% confidence intervals including both statistical and systematic uncertainties. Energies shown are the energy deposited in the detector, assuming that all light emission is from electromagnetic showers. For ν_e charged-current events, this equals the neutrino energy; otherwise, it is a lower limit on the neutrino energy. The gap in E_{dep} between 300 TeV and 1 PeV does not appear to be significant: Gaps of this size or larger appear in 28% of realizations of the best-fit continuous power-law flux.

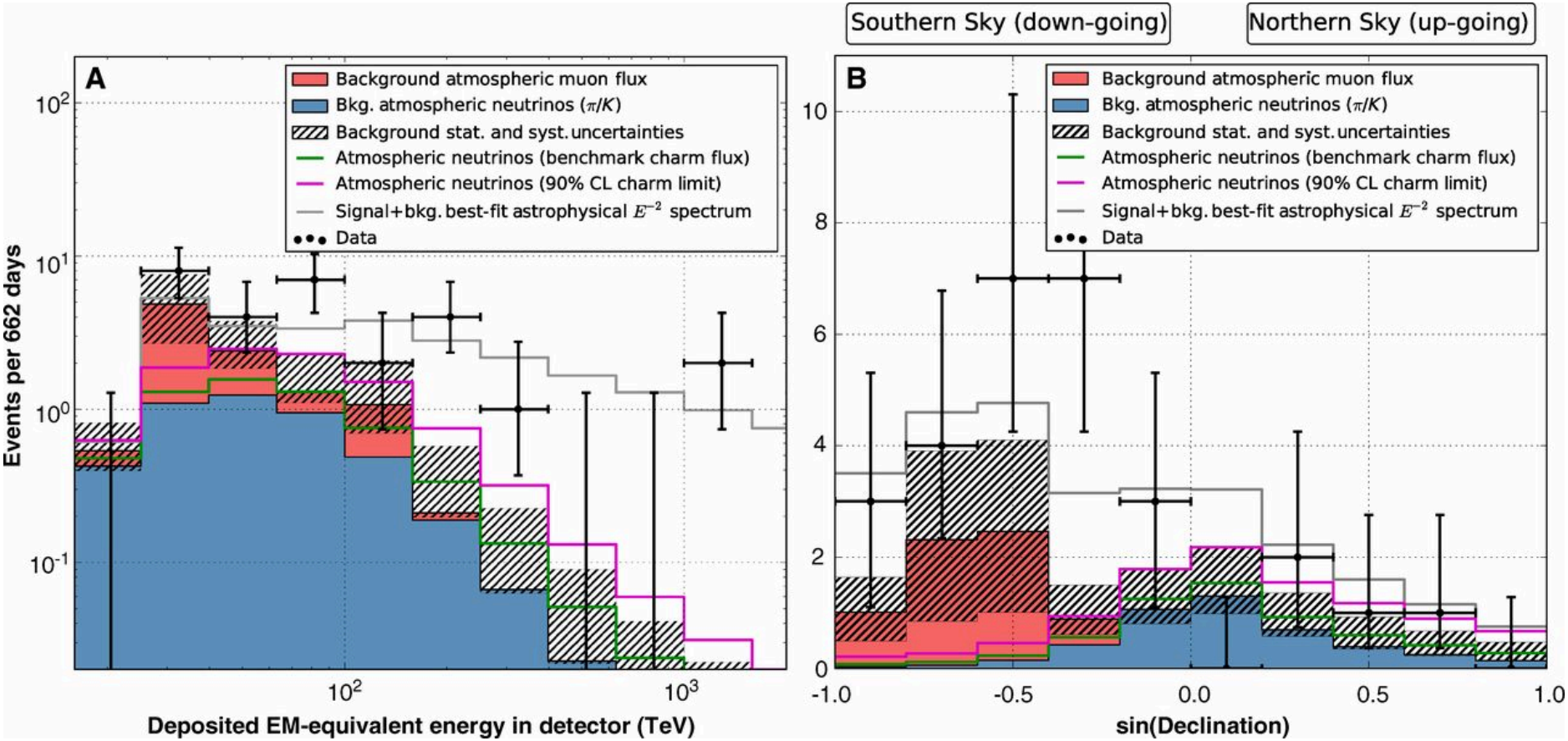

Fig. 4. Distributions of the deposited energies and declination angles of the observed events compared to model predictions.

(**A** and **B**) Zenith angle entries for data (**B**) are the best-fit zenith position for each of the 28 events; a small number of events (Table 1) have zenith uncertainties larger than the bin widths in this figure. Energies plotted (**A**) are reconstructed in-detector visible energies, which are lower limits on the neutrino energy. Note that deposited energy spectra are always harder than the spectrum of the neutrinos that produced them because of the neutrino cross section increasing with energy. The expected rate of atmospheric neutrinos is shown in blue, with atmospheric muons in red. The green line shows our benchmark atmospheric neutrino flux (see the text), and the magenta line shows the experimental 90% bound. Because of a lack of statistics from data far above our cut threshold, the shape of the distributions from muons in this figure has been determined using Monte Carlo simulations with total rate normalized to the estimate obtained from our in-data control sample. Combined statistical and systematic uncertainties on the sum of backgrounds are indicated with a hatched area. The gray line shows the best-fit E^{-2} astrophysical spectrum with a per-flavor normalization (1:1:1) of $E^2\Phi_\nu(E) = 1.2 \times 10^{-8}$ GeV cm^{-2} s^{-1} sr^{-1}.

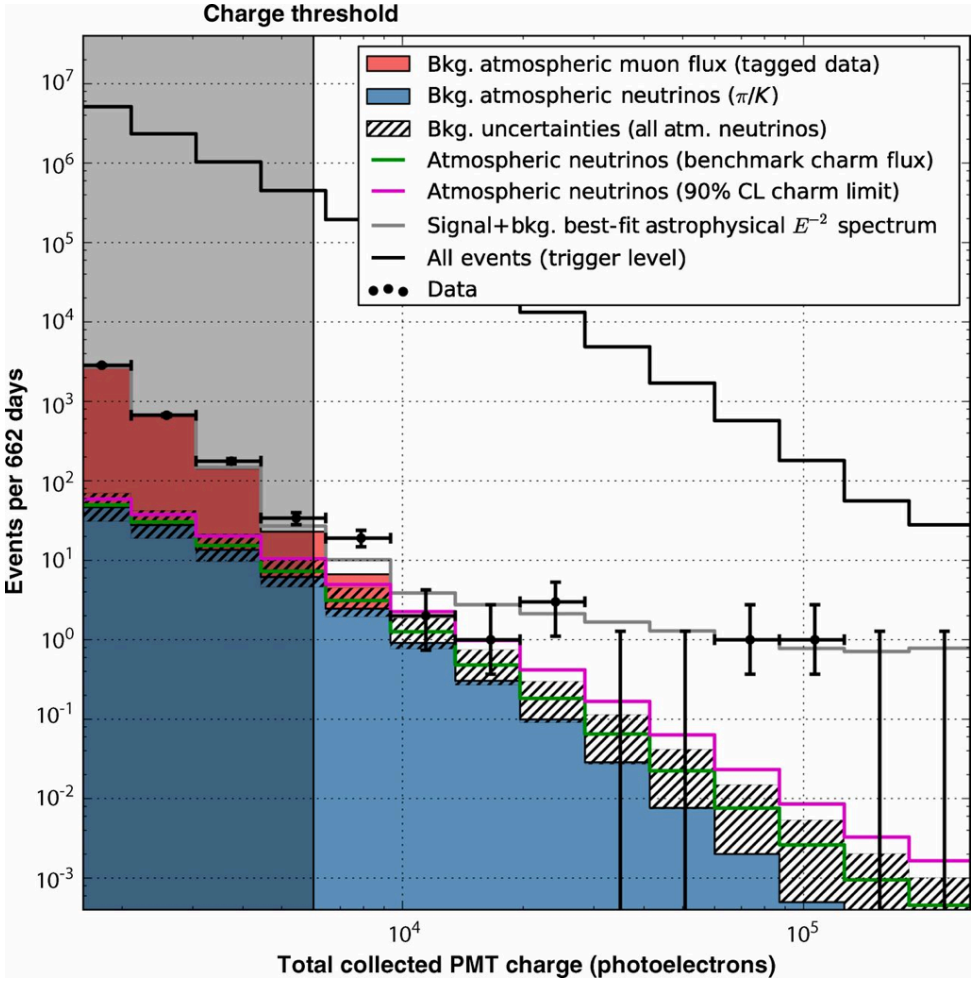

Fig. 6. Distribution of deposited PMT charges (Q_{tot}).

Muons at higher total charges are less likely to pass the veto layer undetected, causing the muon background (red, estimated from data) to fall faster than the overall trigger rate (uppermost line). The data events in the unshaded region, at Q_{tot} > 6000, are the events reported in this work, with error bars indicating 68% Feldman–Cousins intervals. The best-fit E^{-2} astrophysical spectrum (gray line) and atmospheric neutrino flux (blue) have been determined using Monte Carlo simulations, with the hatched region showing current experimental uncertainties on the atmospheric neutrino background. The largest of these uncertainties is neutrinos from charmed meson decays, a flux that has yet to be observed and is thus not included in the blue region; the hatched region includes the best experimental 1σ upper limit (*8*). For scale, two specific charm levels are also shown: a benchmark theoretical model (*6*) (green line) and the experimental 90% CL upper bound (*8*) (magenta line).

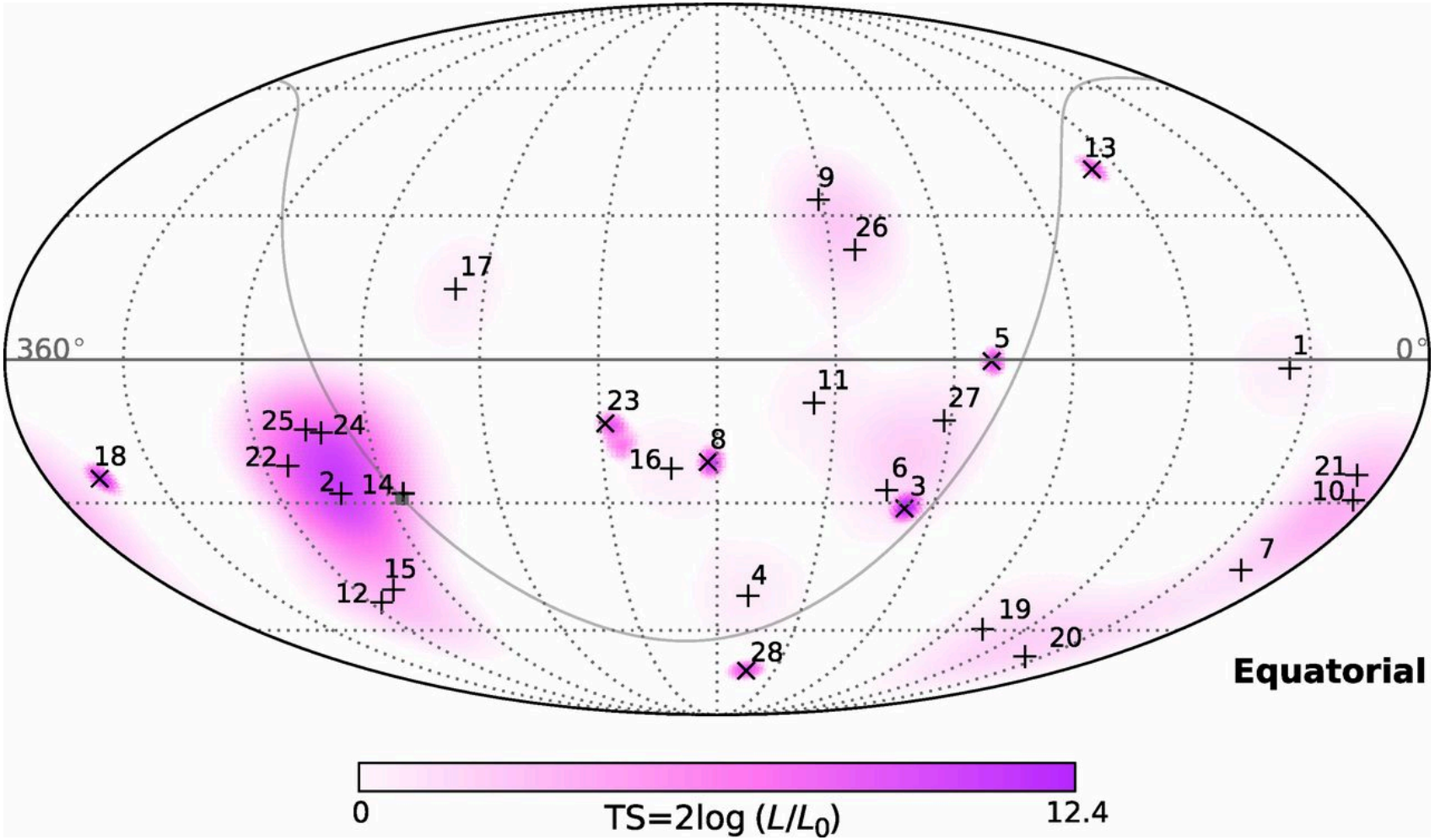

Fig. 5. Sky map in equatorial coordinates of the TS value from the maximum likelihood point source analysis.

The most significant cluster consists of five events—all showers and including the second highest energy event in the sample—with a final significance of 8%. This is not sufficient to identify any neutrino sources from the clustering study. The galactic plane is shown as a curved gray line with the galactic center at the bottom left denoted by a filled gray square. Best-fit locations of individual events (listed in Table 1) are indicated with vertical crosses (+) for showers and angled crosses (×) for muon tracks.

THE ASTROPHYSICAL JOURNAL, 779:132 (17pp), 2013 December 20 doi:10.1088/0004-637X/779/2/132

SEARCH FOR TIME-INDEPENDENT NEUTRINO EMISSION FROM ASTROPHYSICAL SOURCES WITH 3 yr OF IceCube DATA

ABSTRACT

We present the results of a search for neutrino point sources using the IceCube data collected between 2008 April and 2011 May with three partially completed configurations of the detector: the 40-, 59-, and 79-string configurations. The live-time of this data set is 1040 days. An unbinned maximum likelihood ratio test was used to search for an excess of neutrinos above the atmospheric background at any given direction in the sky. By adding two more years of data with improved event selection and reconstruction techniques, the sensitivity was improved by a factor of 3.5 or more with respect to the previously published results obtained with the 40-string configuration of IceCube. We performed an all-sky survey and a dedicated search using a catalog of a priori selected objects observed by other telescopes. In both searches, the data are compatible with the background-only hypothesis. In the absence of evidence for a signal, we set upper limits on the flux of muon neutrinos. For an E^{-2} neutrino spectrum, the observed limits are $(0.9–5) \times 10^{-12}$ TeV^{-1} cm^{-2} s^{-1} for energies between 1 TeV and 1 PeV in the northern sky and $(0.9–23.2) \times 10^{-12}$ TeV^{-1} cm^{-2} s^{-1} for energies between 10^2 TeV and 10^2 PeV in the southern sky. We also report upper limits for neutrino emission from groups of sources that were selected according to theoretical models or observational parameters and analyzed with a stacking approach. Some of the limits presented already reach the level necessary to quantitatively test current models of neutrino emission.

Key words: astroparticle physics – cosmic rays – neutrinos – telescopes

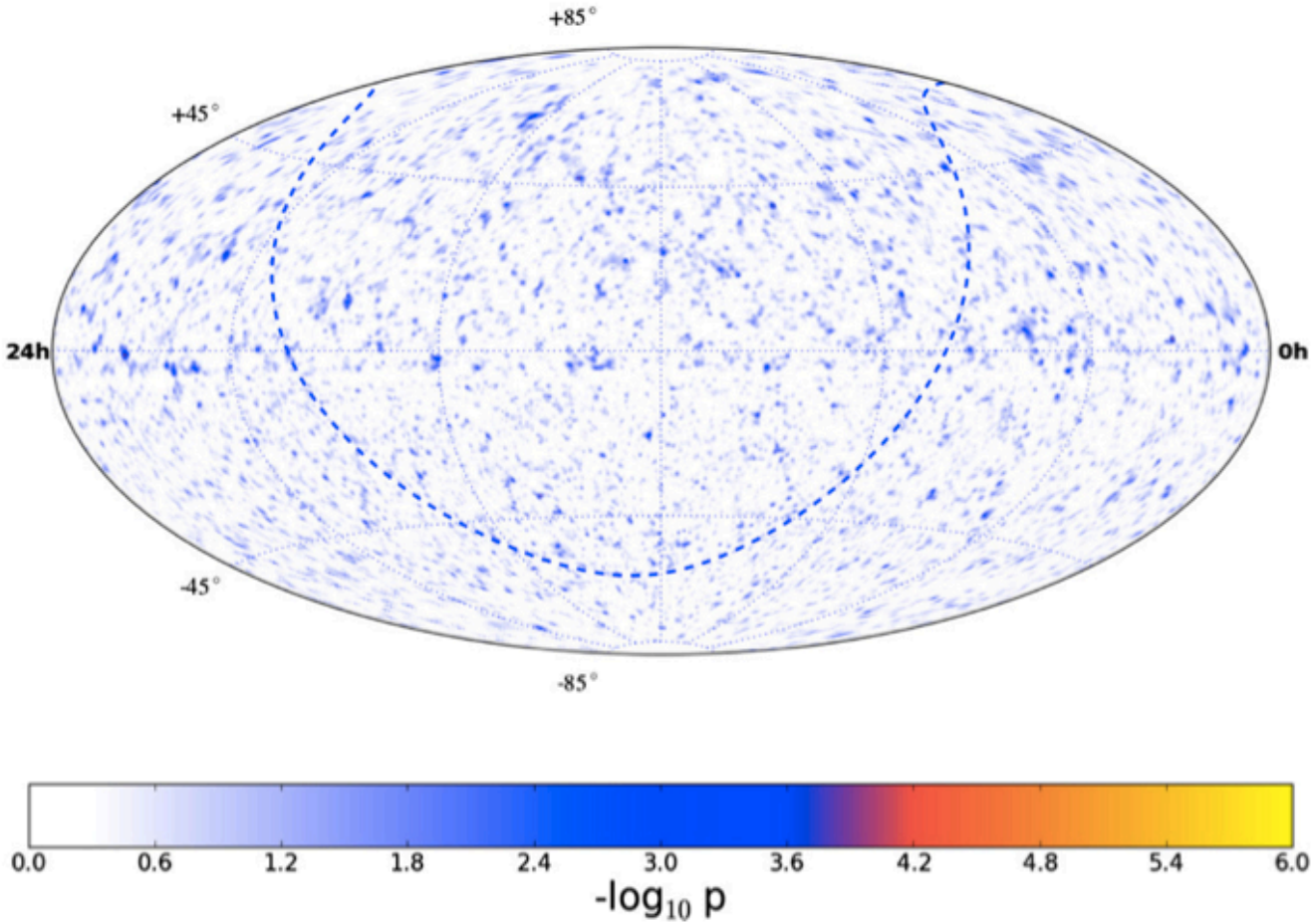

Figure 12. Pretrial significance sky map in equatorial coordinates (J2000) of the all-sky point source scan for the combined IC79 + IC59 + IC40 data sample. The dashed line indicates the Galactic plane.

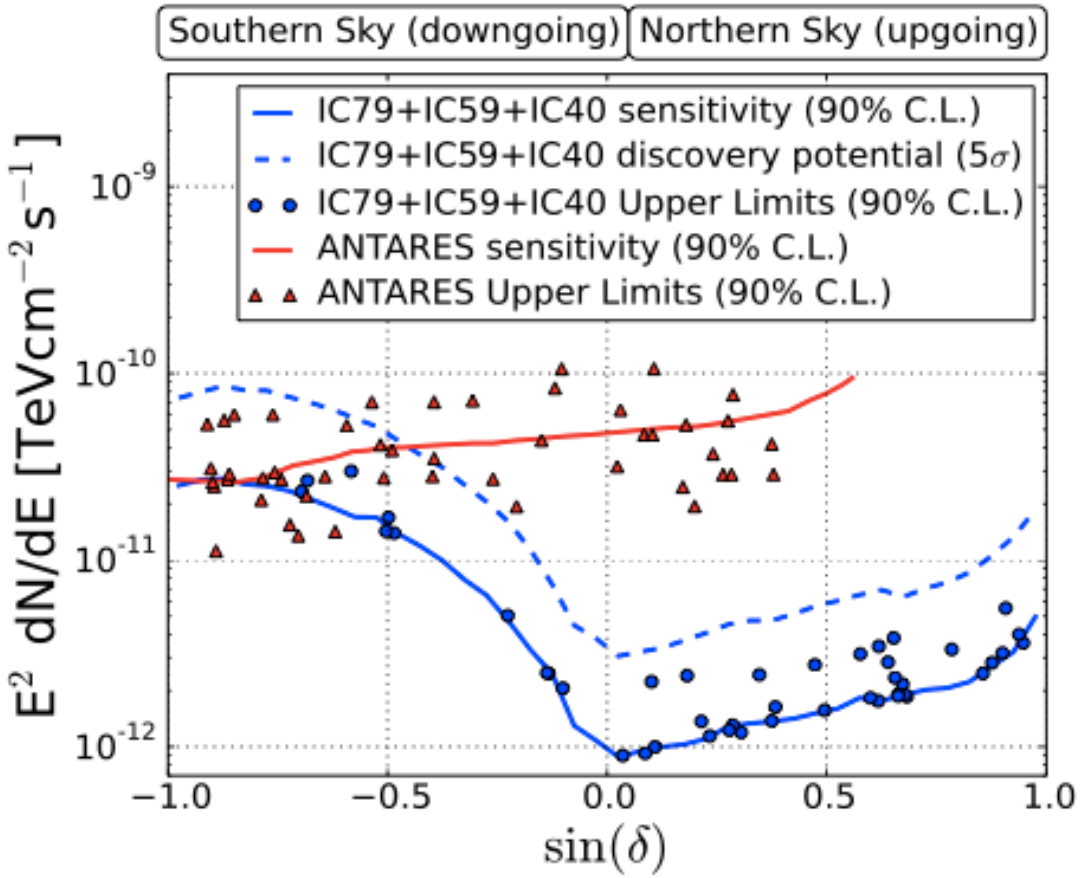

Figure 14. Muon neutrino and antineutrino flux 90% C.L. upper limits and sensitivities for an E^{-2} spectrum for an energy range of 1 TeV to 1 PeV in the northern sky and 10^2 TeV to 10^2 PeV in the southern sky. Published limits of ANTARES (Adrián-Martínez et al. 2011) are also shown. The different likelihood function and method to derive upper limits used by ANTARES may account for differences in the limits from the two experiments at the level of 20%. In the case of the IceCube method, negative values for the number of signal events are not allowed in the minimization procedure. Therefore, for those sources where there was an underfluctuation of the background, the upper limit matches the median upper limit.

Table 2
Results for Galactic Objects on the A Priori Search List

Category	Source	R.A. (°)	Decl. (°)	p-value	$\hat{n}_S$	$\hat{\gamma}$	B_{1°	$\Phi^{90\%}_{\nu_\mu+\bar{\nu}_\mu}$
SNR	TYCHO	6.36	64.18	...	0.0	...	11.1	3.18
	Cas A	350.85	58.81	...	0.0	...	11.5	2.47
	IC443	94.18	22.53	0.43	2.8	3.9	17.2	1.63
	MGRO J1908+06	286.98	6.27	...	0.0	...	23.8	1.00
HMXB/mqso	LSI +63 303	40.13	61.23	...	0.0	...	11.5	2.82
	Cyg X-3	308.11	40.96	0.43	2.5	3.9	12.9	2.35
	Cyg X-1	299.59	35.20	0.21	5.6	3.9	14.6	3.14
	HESS J0632+057	98.25	5.80	0.058[a]	15.6	3.4	24.1	2.23
	SS433	287.96	4.98	...	0.0	...	24.3	0.92
Star Formation Region	Cyg OB2	308.08	41.51	...	0.0	...	12.7	1.87
Pulsar/PWN	MGRO J2019+37	305.22	36.83	...	0.0	...	14.3	1.83
	Crab Nebula	83.63	22.01	...	0.0	...	17.2	1.38
	Geminga	98.48	17.77	...	0.0	...	19.5	1.193
Galactic Center	Sgr A*	266.42	−29.01	0.49	0.6	3.7	25.2	13.94

Notes. Sources are grouped according to their classification as high-mass X-ray binaries or microquasars (HMXB/mqso), SNRs, pulsar wind nebulas (PWNs), and star formation regions. The source MGRO J1908+06 previously considered to be unidentified has been placed in the category of SNR because it is positionally consistent with SNR G40.5−0.5 (Gonzalez-Garcia et al. 2009). The p-value is the pretrial probability of compatibility with the background-only hypothesis. The $\hat{n}_S$ and $\hat{\gamma}$ columns give the best fit number of signal events and spectral index of a power law spectrum. When $\hat{n}_S = 0$, no p-value or $\hat{\gamma}$ is reported. The eighth column gives the number of background events in a circle of 1° around the search coordinates. The last column shows the upper limits based on the classical approach (Neyman 1937) for an E^{-2} flux normalization of $\nu_\mu + \bar{\nu}_\mu$ flux in units of 10^{-12} TeV^{-1} cm^{-2} s^{-1}.
[a] Most significant p-value in the northern sky among all Galactic and extragalactic objects on the a priori search list.

Table 3
Results for Extragalactic Objects on the A Priori Search List

Category	Source	R.A. (°)	Decl. (°)	p-value	$\hat{n}_S$	$\hat{\gamma}$	B_{1°	$\Phi^{90\%}_{\nu_\mu+\bar{\nu}_\mu}$
BL Lac	S5 0716+71	110.47	71.34	...	0.0	...	10.3	3.60
	1ES 1959+650	300.00	65.15	0.19	5.7	3.9	11.1	5.53
	1ES 2344+514	356.77	51.70	0.29	4.7	3.9	12.4	3.32
	3C66A	35.67	43.04	...	0.0	...	12.7	1.86
	H 1426+428	217.14	42.67	...	0.0	...	12.7	1.90
	BL Lac	330.68	42.28	0.42	3.7	3.3	12.7	2.16
	Mrk 501	253.47	39.76	0.34	4.8	3.9	13.4	2.84
	Mrk 421	166.11	38.21	0.18	3.7	1.8	13.7	3.45
	W Comae	185.38	28.23	0.21	2.8	1.8	16.1	2.74
	1ES 0229+200	38.20	20.29	0.19	8.2	3.9	17.8	2.43
	PKS 0235+164	39.66	16.62	...	0.0	...	19.9	1.30
	PKS 2155−304	329.72	−30.23	...	0.0	...	25.5	14.28
	PKS 0537−441	84.71	−44.09	...	0.0	...	23.8	23.27
FSRQ	4C 38.41	248.81	38.13	...	0.0	...	13.7	1.76
	3C 454.3	343.49	16.15	...	0.0	...	19.9	1.23
	PKS 0528+134	82.73	13.53	...	0.0	...	20.8	1.14
	PKS 1502+106	226.10	10.49	0.076	8.4	2.3	21.2	2.40
	3C 273	187.28	2.05	...	0.0	...	25.0	0.90
	3C279	194.05	−5.79	...	0.0	...	23.5	2.06
	QSO 2022−077	306.42	−7.64	...	0.0	...	23.2	2.47
	PKS 1406−076	212.24	−7.87	...	0.0	...	23.2	2.49
	QSO 1730−130	263.26	−13.08	...	0.0	...	25.6	5.04
	PKS 1622−297	246.53	−29.86	0.45	0.7	4.0	25.2	16.91
	PKS 1454−354	224.36	−35.65	0.23[a]	1.0	5.9	24.1	29.89
Starburst	M82	148.97	69.68	...	0.0	...	10.7	4.00
Radio galaxies	NGC 1275	49.95	41.51	...	0.0	...	12.7	1.91
	Cyg A	299.87	40.73	0.15	1.5	1.5	12.9	3.82
	Cen A	201.37	−43.02	0.46	2.0	1.4	23.9	26.62
	3C 123.0	69.27	29.67	...	0.0	...	15.9	1.57
	M87	187.71	12.39	0.45	2.9	...	20.9	1.37

Notes. Sources are grouped according to their classification as BL Lac objects, radio galaxies, flat-spectrum radio quasars (FSRQ), and starburst galaxies. The p-value is the pretrial probability of compatibility with the background-only hypothesis. The $\hat{n}_S$ and $\hat{\gamma}$ columns give the best fit number of signal events and spectral index of a power law spectrum. When $\hat{n}_S = 0$, no p-value or $\hat{\gamma}$ is reported. The eighth column gives the number of background events in a circle of 1° around the search coordinates. The last column shows the upper limits based on the classical approach (Neyman 1937) for an E^{-2} flux normalization of $\nu_\mu + \bar{\nu}_\mu$ flux in units of 10^{-12} TeV^{-1} cm^{-2} s^{-1}.

[a] Most significant p-value in the southern sky among all Galactic and extragalactic objects on the a priori search list.

Astroparticle Physics at the Department of Astrophysics RU Nijmegen

- **Charged cosmic rays**
  LOPES, LOFAR, Pierre Auger Observatory **(Falcke, Hörandel)**
  TRACER, KASCADE-Grande **(Hörandel)**
- **Acceleration of high-energy particles** **(Achterberg)**
- **Gamma ray astronomy - CTA** **(Hörandel)**
- **Gravitational waves - LISA, VIRGO** **(Nelemans, Groot)**
- **Magnetic fields in the Galaxy** **(Haferkorn)**